J Mater Sci (2021) 56:14416–14447

Review

Strategies to improve WO_3-based photocatalysts for wastewater treatment: a review

Meiju Liao[1], Long Su[1], Yaocheng Deng[1,*], Sheng Xiong[1], Rongdi Tang[1], Zhibin Wu[1], Chunxia Ding[2], Lihua Yang[1], and Daoxin Gong[1]

[1] College of Resources & Environment, Hunan Agricultural University, Changsha 410128, China
[2] School of Chemistry and Materials Science, Hunan Agricultural University, Changsha 410128, China

Received: 27 November 2020
Accepted: 21 May 2021
Published online: 9 June 2021

ABSTRACT

WO_3, a visible light reaction catalyst, absorbs light at a wavelength of 470 nm and has many advantages, such as strong stability, long life, non-toxicity, low cost, and suitable band edges. In this review, the photocatalytic mechanism of WO_3 in water pollution treatment is introduced, as well as a systematic summary, and some main strategies for improving the photocatalytic activity of WO_3 in water pollution treatment are introduced, for example surface and morphology control, synthetic heterojunctions, and doping element. Finally, the main conclusions and prospects of WO_3-based photocatalysts are pointed out. It can be expected that this review can provide guidance for designing low-cost, high-efficiency new WO_3-based photocatalysts in the process of water pollution treatment and can meet the application prospects of efficient utilization of solar degradation in the field of environmental purification.

Handling Editor: Mark Bissett.

Meiju Liao and Long Su contributed equally to this work.

Address correspondence to E-mail: dengyaocheng@hunau.edu.cn

https://doi.org/10.1007/s10853-021-06202-8

GRAPHICAL ABSTRACT

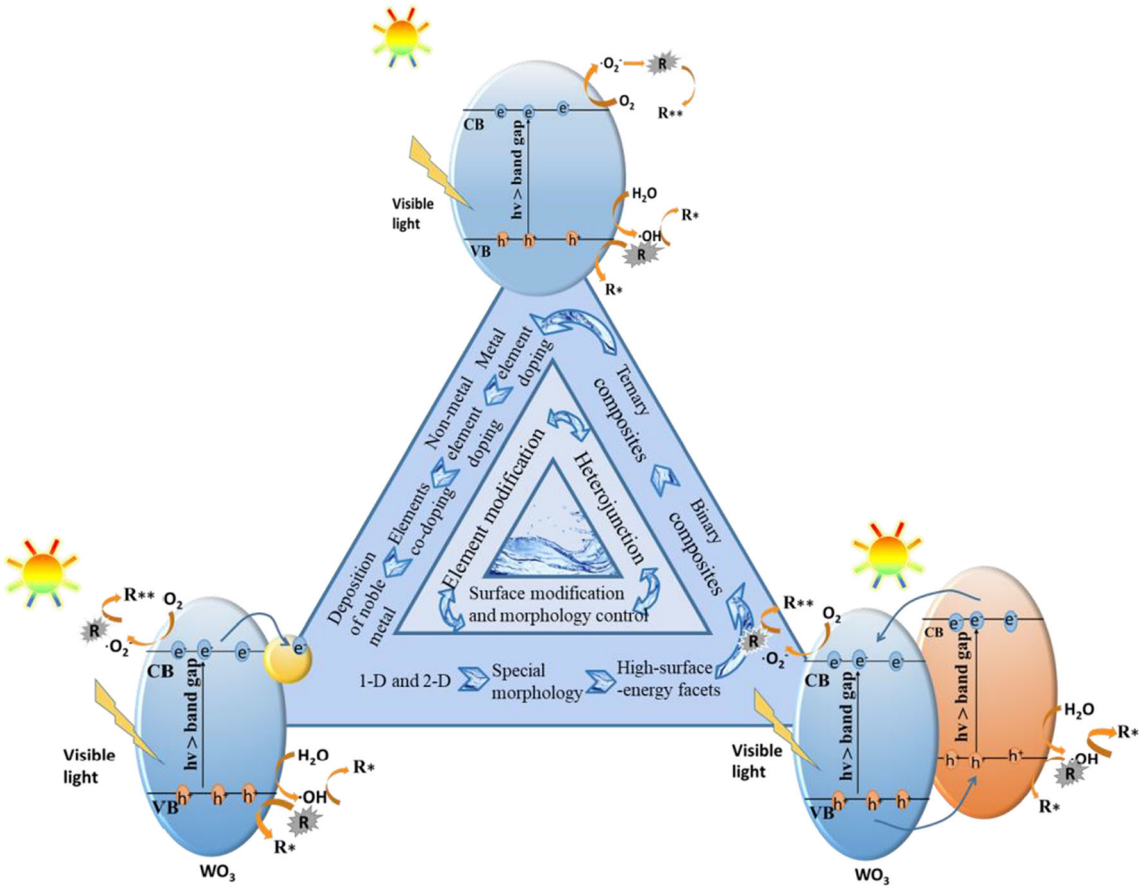

Abbreviations

ROS	Reactive oxygen species
VB	Valence band
CB	Conduction band
RhB	Rhodamine B
MB	Methylene blue
MO	Methyl orange
ER	Eosin red
CR	Congo red
GR	Graphene
GO	Graphene oxide
RGO	Reduced graphene oxide
RhB 6G	Rhodamine B 6G
TC	Tetracycline
BF	Basic fuchsin
IC	Indigo carmine
SMX	Sulfamethoxazole
CV	Crystal violet
AO_7	Acid orange 7
TOC	Total organic carbon
SAM	Sulfanilamide

Introduction

With the rapid development of modern society and the industrialization process, water environmental pollution has become the focus of attention. It is imperative to find a suitable and effective treatment

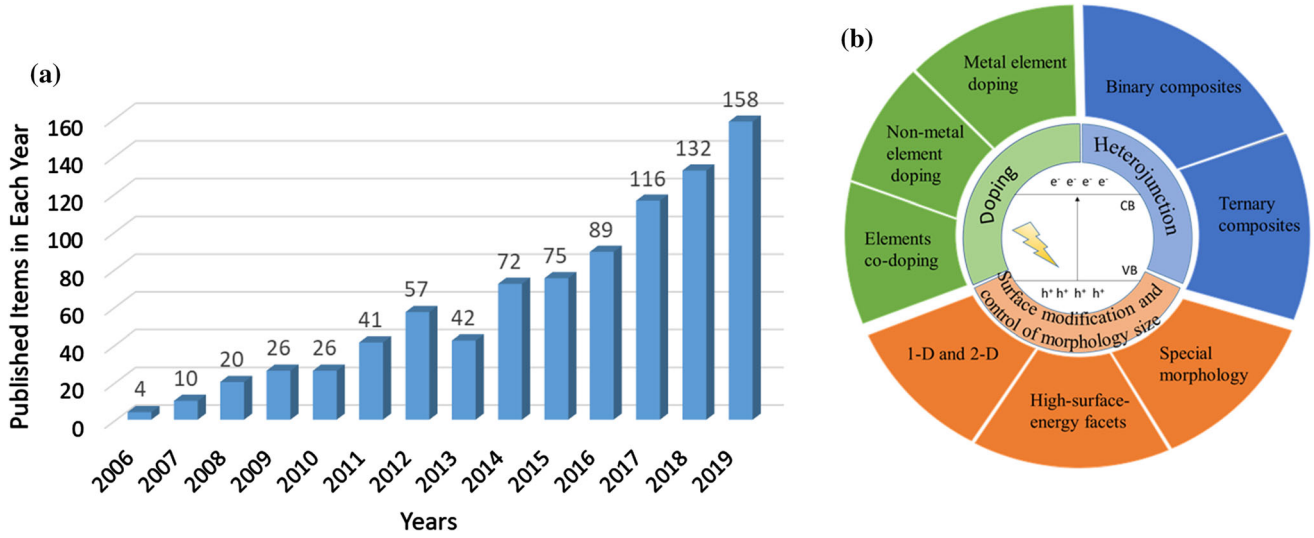

Figure 1 **a** The Number of Journal Citation Reports (JCR) articles per year, as reported by Web of Science (http://apps.webofknowledge.com) from 2006 and updated to December 2019 retrieved via the keywords "WO_3" and "photocatalysis" in the topic of papers. **b** The mechanism of WO_3 and strategies for enhancing the photocatalytic activity of WO_3 photocatalysts in wastewater.

method. In the past few decades, the application of photocatalysis has attracted attention because it can be widely used in many fields, especially in the environment and energy fields [1, 2]. Photocatalysis is an effective treatment method for degradation of persistent organic trace pollutants because the photocatalyst is stimulated by effective light to generate photo-generated electrons and holes, thereby causing O_2 and H_2O to generate active oxygen species (ROS, such as $\cdot OH$, $\cdot O_2^-/\cdot HO_2$, H_2O_2,$_1O_2$) to degrade the pollutants [3]. Part of the research on reactive oxygen species can also inactivate some microorganisms.

Among many photocatalysts, TiO_2 has been the most widely studied due to its non-toxicity, availability, and low price [4]. Since the water was first demonstrated to decompose into H_2 on TiO_2 photoanode [5], it is one of the most widely used photocatalysts at present due to the overall superior properties of TiO_2, including availability, long-term stability, and non-toxicity [6]. However, TiO_2 only can respond to about 4% of solar ultraviolet radiation with large band-gap energy ($\sim$ 3.2 eV) [7]. Also, the fast electron–hole recombination inherent in conventional TiO_2 photocatalysts is an important factor affecting its low photocatalytic efficiency.

Recently, tungsten trioxide (WO_3) has attracted attention due to its strong ability to degrade organic pollutants, high stability, long life, non-toxicity, low cost, and suitable band edges. Since it was first reported in 1976, extensive research has been conducted on the photocatalytic performance of WO_3. Especially in the past ten years, a great deal of research has focused on WO_3 and improving WO_3 photocatalytic performance. In Fig. 1a, the rising trend indicates that the application of WO_3 photocatalyst in the field of photocatalysis is increasing.

Over the past several decades, photocatalysis has been the best procedure for wastewater treatment because of the ability of this method to perfectly mineralize the contaminants. In 1976, Butler et al. already reported that *n*-type tungsten trioxides were a great photocatalyst for water oxidation [8]. Because of the narrow band-gap (2.6–2.8 eV), nontoxicity, and strong adaptability of WO_3, it has considered as a photocatalyst that can effectively degrade pollutants [9]. The valence band (VB) of WO_3 was about 3.1 eV [10], which made WO_3 have a strong oxidizing property. The mechanism of WO_3 is shown in Fig. 1b.

The large specific surface area of WO_3 nanostructure can increase the effective surface area of photocatalytic reaction. However, there are also materials with larger surface areas showing lower photocatalytic activity. For example, some scholars have pointed out that 500 nm WO_3 nanoparticles obtained at 800 °C can induce more O_2 precipitation than 30 nm nanoparticles obtained at 500 °C [11], which is

attributed to the fact that larger particles have better crystallinity (resulting in smaller Eg), and thus counteracting the effect of small specific surface area [12]. In addition to the above effects, the range of photo-response values and the recombination speed of photogenerated carriers will affect the WO_3 photocatalytic performance. Therefore, some strategies which can change the WO_3 photo-response value and photogenerated carriers recombination efficiency are adopted to enhance the photocatalytic activity of WO_3. So far, strategies for improving the photocatalytic performance of WO_3 for contaminants, i.e., surface modification and control of morphology size, synthetic heterojunction, element doping, are being reported. We need a review to summarize the improvement of photocatalysts based on WO_3 in wastewater treatment. In this review, the photocatalytic mechanism of WO_3 and three aspects to enhance the photocatalytic activity of WO_3 in water pollution are introduced. Finally, the research status and application challenges of WO_3-based photocatalysts are briefly summarized.

Advantages and limitations of pure WO_3 in photocatalysis

As a photocatalytic material, it is impossible to oxidize H_2/H_2O (relative to NHE (common hydrogen electrode)) and reduce H_2O/O_2 due to the positions of the conduction band (CB) and valence band (VB) of the WO_3 semiconductor. These allow WO_3 to effectively degrade many organic compounds, such as textile dyes and antibiotics [12–14], which can also inactivate some microorganisms [15]. Besides, WO_3 has significant stability in acidic environments and is an excellent material for treating organic acid contaminated water [16]. And some advantages are mentioned in the previous section, such as high stability, long life, non-toxicity, low cost, suitable band edges, and so on.

The photocatalyst absorbs energy from optical radiation to generate hole and electron pairs. Then, holes and electrons directly react with pollutants or generate free radicals and degrade pollutants through oxidation and reduction reactions. Therefore, the position of the energy level between VB and CB and the band-gap of WO_3 play a decisive role in

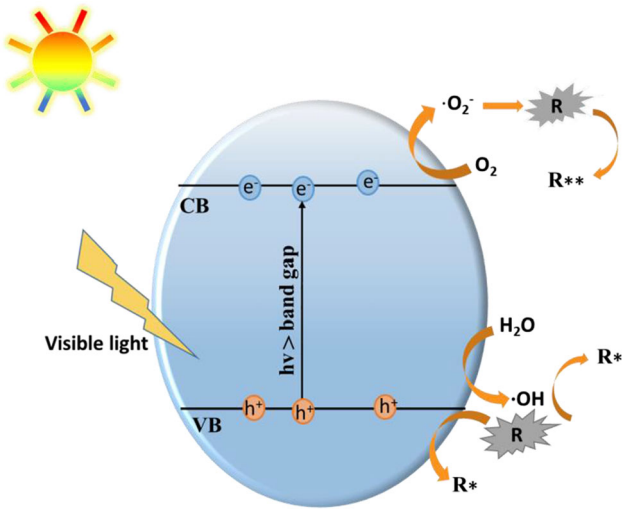

Figure 2 Mechanism of WO_3 degradation of pollutants.

the ability to oxidize and reduce pollutants. Figure 2 shows the photocatalytic mechanism of the WO_3 semiconductor. The reactions are as follows:

$$\text{Photocatalyst} + \text{hv} \rightarrow e^- + h^+ \quad (1)$$

$$H_2O \rightarrow H^+ + OH^- \quad (2)$$

$$e^- + O_2 \rightarrow \cdot O_2^- \quad (3)$$

$$h^+ + OH^- \rightarrow \cdot OH \quad (4)$$

$$\cdot OH/h^+ + R\ (\text{pollutant}) \rightarrow R*(\text{oxidized}) \quad (5)$$

$$\cdot O_2^- + R \rightarrow O_2 + R**(\text{reduced}) \quad (6)$$

$$R*(\text{oxidized}) \text{ or } R**(\text{reduced}) \rightarrow (\text{final products}) \rightarrow CO_2 + H_2O \quad (7)$$

The free radicals generated are the key to the degradation of organic pollutants. However, four important effects limit the photocatalytic performance of tungsten trioxides for wastewater treatment: first of all, low visible light response ability ($\lambda < 470$ nm); secondly, low specific surface area; thirdly, fast recombination rate of photogenerated electron–hole pairs [17]; fourthly, many reactions in photocatalysts cannot happen due to the low CB position (low than −0.1 V vs NHE, PH = 7), for example single-electron reduction of O_2 ($O_2 + e^- \rightarrow O_2^-$(aq), −0.33 V) and reduction of H^+ to H_2 ($2H^+ + 2e^- \rightarrow H_2$, −0.41 V) [18]. Therefore, for the WO_3 semiconductor without any improvement, its photocatalytic activity is relatively low. In the recent

Table 1 Modification for enhancing the photocatalytic activity by using various shapes WO_3 photocatalyst

Material	Pollutant	Concentration of pollutant	Method	Light source	Bandgap value	Results	Ref
1-D and 2-D structures							
Nanoparticles	MB	–	Inverse microemulsion	visible-light	2.88 eV	75% in 90 min	[47]
Nanorods	MB	10 ppm	Hydrothermal method	800 W Xe lamp	2.75 eV	93.1% in 70 min	[22]
	ER	10 ppm				86% in 70 min	
	CR	10 ppm				87% in 80 min	
Nanofibers	MB	20 ppm	Simple electrospun method	visible-light	–	50% in 120 min	[24]
Nanosheets	MB	20 ppm	The means of thermal deposition		–	MB adsorption capacity can reach 600 mg/g	[32]
Nanoplates	MB	10 ppm	PABA-assisted hydrothermal method	Xe lamp at 400 nm	–	~98.12% in 60 min	–
	RhB	5 ppm	Hydrothermal method	Xe lamp at 400 nm	2.63 eV	100% in 150 min	[48]
Films	RhB	47.9 ppm	Simple chemical spray pyrolysis technique	Solar radiation	2.64 eV	12% in 160 min	[30]
Special morphology							
WO_3 hollow microspheres	RhB	4.79 ppm	Hydrothermal method	Visible-light	2.7 eV	–	[36]
WO_3 flower-like	MB	10 ppm	Straightforward hydrothermal method	300 W Xe lamp	2.55 eV	94.7% in 60 min	[37]
WO_3 cylindrical stacks	MB	10 ppm	Straightforward hydrothermal method	300 W Xe lamp	2.58 eV	90.3% in 60 min	[37]
Flower-like $WO_3 \cdot 0.33H_2O$	RhB	10 ppm	Hydrothermal method	500 W high-pressure UV mercury lamp		≈78% in 60 min	[38]
Hierarchical WO_3 structures	MB	10 ppm	A facile and surfactant-free hydrothermal method	800 W Xe lamp		92% in 110 min	[42]
	ER	10 ppm				81% in 110 min	
	CR	10 ppm				75% in 110 min	
3D hierarchical $WO_3 \cdot 0.33H_2O$	RhB	10 ppm	One-pot solvothermal method	300 W Xe lamp		92% in 50 min	[40]
Hierarchical WO_3 core–shell	RhB	10 ppm	Template-free precipitation method	Visible light		75% in 120 min	[41]

years, many strategies have been proposed, which can improve the activity of WO_3 photocatalyst. Therefore, in Sect. 3, we will elaborate on the following points, such as surface modification and morphological size control, the formation of heterojunctions and the modification of other elements.

Strategies for improving photocatalytic activity of WO_3 for wastewater treatment

Surface modification and control of morphology size of WO_3 for wastewater treatment

Surface modification and morphology control of photocatalysts are generally regarded as effective strategies to enhance the activity of photocatalysts because the crystal surface and morphology can be changed. Besides, the shape of the material will affect the photocatalytic activity of WO_3 nanostructures to a certain extent [19]. Therefore, surface modification and morphology control of WO_3 nanostructures are very important for efficient photocatalytic degradation of water pollutants.

WO_3 one-dimensional structures and two-dimensional structures

One-dimensional (1-D) semiconductor structures can provide a direct path for photo-generated charges transfer, have small grain boundaries and thus own excellent charge transport properties. Since the scattering of free electrons is suppressed, the photocatalytic activity of one-dimensional nanomaterials can be improved compared to nanoparticles [20]. In the recent years, various one-dimensional WO_3 nanostructures have been developed, such as nanorods [21–23], nanofibers [24], nanotubes [25], and nanowires [26]. Table 1 shows the effects of various WO_3 one-dimensional structures and two-dimensional shapes on wastewater treatment. For example, nanofibers have excellent porosity, excellent mechanical and ideal chemistry property, which can improve the photocatalytic activity of WO_3. It has

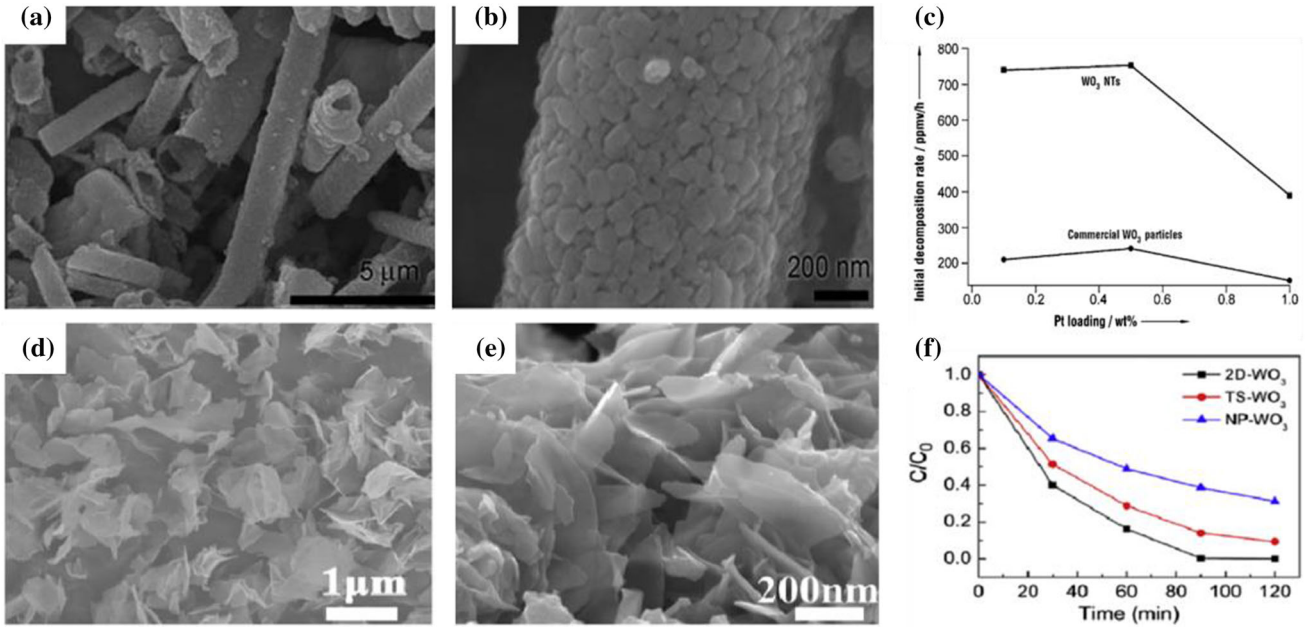

Figure 3 **a** and **b** SEM images with WO_3 NTs. **c** Plots of initial decomposition rates versus Pt-loading concentration (adapted with permission from reference [27]. Copyright (2008) Wiley–VCH). **d** and **e** SEM images with different magnification of 2D-WO_3. **f** Change of MO normalization concentration versus the exposure time under irradiation with the different photocatalysts (adapted with permission from reference [33], Copyright (2019) Elsevier).

been reported that WO_3 nanofibers were prepared by electro-spinning, which degraded methylene blue twice as efficiently as WO_3 particles [24]. Compared with nanofibers, nanotubes can provide higher surface area and more effective sites to degrade pollutants, so that pollutant molecules can be diffused quickly and effectively in nanotube structures. For example, Zhao et al. successfully synthesized WO_3 nanotubes through template-free WCl_6 urea-assisted alcoholysis and the SEM images are shown in Fig. 3a–b [27]. These WO_3 NTs are monodisperse, with a diameter of about 300–1000 nm and a length of about 2–20 mm. They are composed of a single WO_3 nanoparticle linear arrangement, and many self-supporting pores are formed due to incomplete aggregation of the nanoparticles. Experiment results show that the BET value of these WO_3 NTs (25 m^2g^{-1}) is increased by 5.7 times, compared with the BET value of commercial WO_3 particles (4.4 m^2g^{-1}), and that WO_3 NTs can generate electron–holes in visible light with a wavelength greater than 400 nm. Compared with commercial WO_3 particles, the prepared nanotubes have higher RhB degradation efficiency and better photocatalytic performance. The relationship between the initial decomposition rate of the two materials and the Pt loading concentration is shown in Fig. 3c. Because the tubular structure has larger effective surface area, higher charge carrier mobility, and wider light response range, the degradation activity of the nanotube is enhanced. Different shapes of the one-dimensional WO_3 structure have their own advantages, and can be selected according to the purpose in order to degrade the pollutants efficiently and cheaply.

Unlike one-dimensional materials, two-dimensional materials are nano-flaky materials with flat surfaces and high aspect ratios, with an extremely small thickness and strong adhesion to substrates. Nanosheets [28], nanoplates [29] and films [30, 31] have been developed. Research has shown that by using WO_3 nanosheet as the adsorbent, the saturated adsorption amount can reach MB 600 mg/g, higher than the normally activated carbon powder [32]. Due to the high adsorption capacity, the photocatalytic performance of the nanosheets is improved. Compared with ordinary two-dimensional nanosheets, ultrathin nanosheets have the advantages of greater specific surface area and richer active sites, which make WO_3 ultrathin nanosheets present better catalytic performance. For example, Liang et al.

synthesized a two-dimensional (2D) ultrathin WO_3 nanosheet dominated by {002} crystal plan through a simple surfactant-induced self-assembly method and the SEM images of 2D-WO_3 are shown in Fig. 3d–e [33]. The SEM diagram shows the ultra-thin nanosheet structure with a lateral dimension of hundreds of nanometers and a thickness of about 4.9 nm. The experimental results show that the degradation rate constant of MO by 2D-WO_3 is 6.5 times higher than that of WO_3 nanoparticles, showing strong degradation activity (Fig. 3f). The improvement in properties can be owned to the 2D-WO_3 with unique structure, such as high reactivity {002} crystal surface percentage, high specific surface area, wide photo-response range, and high photogenerated electron–hole separation rate. It can be seen that WO_3 two-dimensional materials show superiority in degrading pollutants.

Based on the synthesized one-dimensional and two-dimensional WO_3 nanomaterials, the degradation efficiency of the photocatalyst can be further improved by other methods. Here, we only give a brief example by adding oxygen vacancies on the surface of the materials. For example, Wang and his colleagues synthesized uniformly distributed oxygen vacancies on the surface of WO_3 nanorods through the hydrothermal method [21]. The performance of WO_3 nanorods photocatalyst was demonstrated by comparing with the efficiency of alcohol oxidation to the corresponding ketone. The experimental results show that the activity of WO_3 nanorods prepared by this method is greatly improved, through the adsorption of alcohol molecules with higher specific surface area, the rapid transfer of photogenerated electrons with smaller crystal size, and the surface oxygen vacancies as traps to capture photoelectrons, thus reducing the recombination of photoelectrons and holes. The author believes that the combined effect of the above three points improves the photocatalytic performance of WO_3. Also, Wu et al. successfully synthesized WO_3 ultra-thin nanosheets with oxygen vacancies on the surface [34]. The improvement of the material in photocatalysis is similar to the nanorods appealed. Some studies call the addition of oxygen vacancies as self-doped, which means the dope of oxygen vacancies on the surface of the material. For example, Wang and his colleagues used electrochemical methods to add oxygen holes to the surface of WO_3/TiO_2 heterojunction to improve the degradation of exhaust gas [35].

Compared with pure WO_3, the photocatalytic activity of different shapes of WO_3 has been improved to some extent, but the comparison between different shapes is not clear. In 2014, Farhadian et al. have prepared and characterized one-dimensional WO_3 nanostructures and two-dimensional WO_3 nanosheets, i.e., nanorods, nanosphere, and nanoplates, to study the photocatalytic performance of the shape on the degradation of RhB dye, as displayed in Fig. 4 [19]. In this experiment, the authors found that tetrahedral and cubic nanostructures (nanorods and nanoplates) had higher catalytic activity than spherical nanostructures (nanosphere) because they had more atoms at the edges and corners and these atoms showed higher catalytic activity. Therefore, nanoplates and nanorods had a stronger adsorption capacity than nanosphere. However, the band-gap of WO_3 nanorods in this experiment was the same as the band-gap of TiO_2, so it has a very low light response range in visible light. The results show that nanoplates have the highest degradation performance among the three shapes. Similarly, R. Narayanan et al. studied the effect of different shaped materials on photocatalytic activity in 2004, which was consistent with this conclusion. So we can see that different shapes of WO_3 materials can affect the band-gap, specific surface area, and adsorption capacity. Through this experiment, it can be seen that different shapes of WO_3 materials can also affect the activity of atoms.

Special morphology

Other different shapes can increase the photocatalytic activity of pure WO_3 in water pollution treatment through measures such as increasing specific surface area, improving separation efficiency, and enhancing light response. Some scholars have reported that other shapes have been synthesized but mainly composed of WO_3 nanoparticles, nanorods, and nanosheets. Hollow particles (Fig. 5a) [36] and flowers (Fig. 5b) [37] are composed of nanoparticles. The nanorods can form cylindrical stacks (Fig. 5c) [37] and a flower shape (Fig. 5d) [38]. A flower-like structure is formed by most nanosheets stacked closely together (Fig. 5e) [39], and a $WO_3{\cdot}0.33H_2O$ microsphere structure is formed by nanosheets stacked (Fig. 5f) [40]. The core layer is a dense structure composed of aggregated nanoparticles, and the shell layer is a layered structure composed of

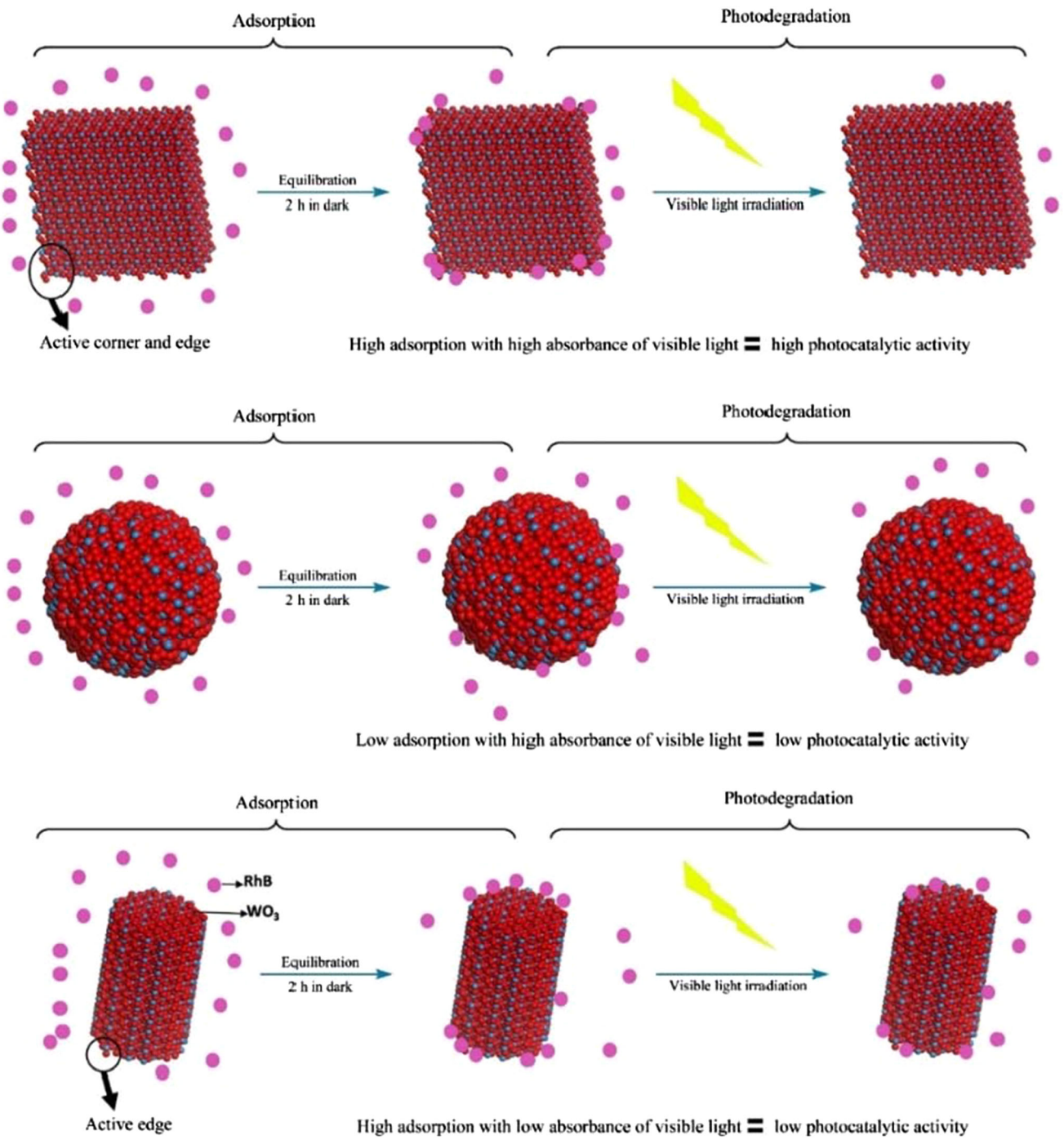

Figure 4 Schematic illustration of the shape effect on the photocatalytic activity of the WO_3 nanostructures (adapted with permission from reference [19], Copyright (2015) Elsevier).

WO_3 ultra-fine nanoplates [41]. Table 1 shows the effects of various WO_3 special morphology shapes on wastewater treatment.

For example, Xu and his colleagues successfully synthesized three-dimensional flower-like and wheel-like structures based on one-dimensional WO_3 nanorods (Fig. 5d) [38]. Due to the high charge separation efficiency of wheel-shaped and flower-shaped WO_3, the degradation activity of RhB was improved.

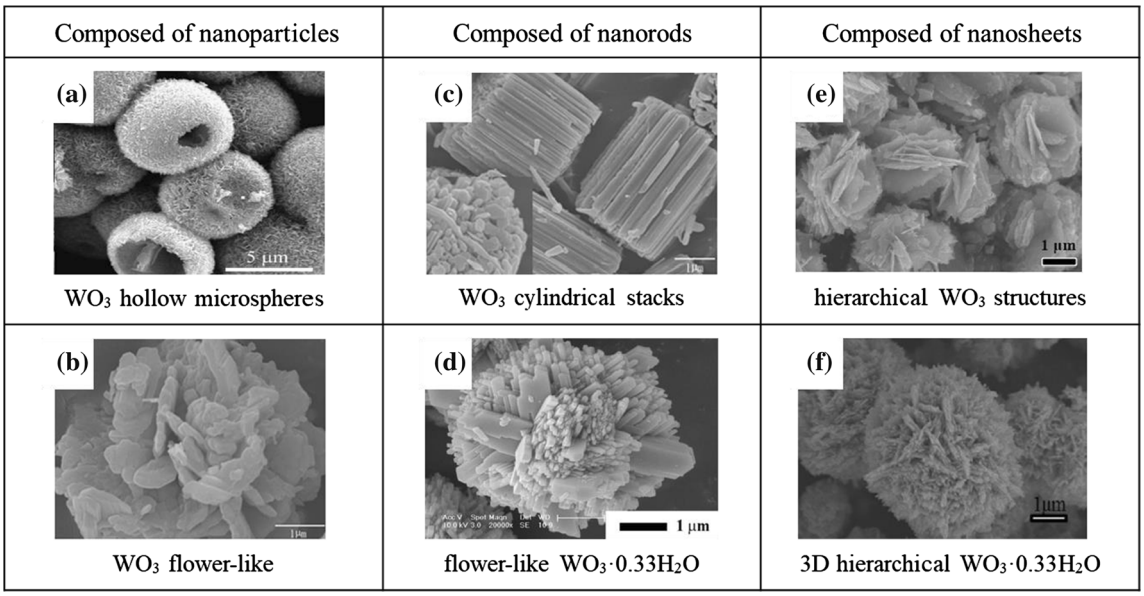

Figure 5 SEM images of **a** WO_3 hollow particles (adapted with permission from reference [36], Copyright (2008) Elsevier); **b** WO_3 flower-like and **c** WO_3 cylindrical stacks (adapted with permission from reference [37], adapted with permission from reference); **d** flower-like $WO_3{\cdot}0.33H_2O$ (adapted with permission from reference [38], Copyright (2014) American Chemical Society); **e** hierarchical WO_3 structures (adapted with permission from reference [42], Copyright (2016) Elsevier) and **f** 3D hierarchical $WO_3{\cdot}0.33H_2O$ (adapted with permission from reference [40], Copyright (2017) Elsevier).

Because after irradiation with appropriate wavelength, the generated holes migrate to the surface along the potential slope generated by the bending of the band, and are captured by the H_2O molecules adsorbed on the surface of $WO_3{\cdot}0.33H_2O$, thereby generating hydroxyl radicals ·OH and reducing the photogenerated electron–hole recombination. The larger photo-response range and longer photo-carriers existing time make the material have better photocatalytic performance. Another example is the WO_3 layered structure composed of WO_3 nanosheets; Yao et al. synthesized WO_3 nanosheets by a simple and surfactant-free hydrothermal method and combined them into WO_3 layered structure (Fig. 5f) [42]. The effect of this material on the degradation of MB, ER and CR harmful organic dyes was studied under simulated sunlight. The results show that the layered WO_3 nanostructures have more excellent water pollutant degradation efficiency. Besides, by changing different raw materials, different WO_3 shapes can be obtained, thereby enhancing the degradation of pollutants by WO_3. For example, the calcined acid-treated $PbWO_4$ (sacrifice template) can obtain dendritic and spherical morphology, while $SrWO_4$ can observe dumbbells [43].

In general, the larger specific surface area will have the greater the number of reaction sites. The synthesized spheres and flowers have a higher specific surface area, so the photocatalytic performance of pure WO_3 is improved to a certain extent. The research and control of different morphologies show that the morphology of photocatalysts is very important in the development of its increased activity. Because these reactions are usually completed on the surface, it depends to a large extent on the morphology of the surface. Compared with general commercial WO_3, the material composed of tiny single crystals has a larger surface area, higher light transmittance, and more active sites, and thus has higher photocatalytic activity. This provides an idea for the preparation of WO_3 structures with stronger photocatalytic degradation ability in the future.

WO_3 high-surface-energy facets

In some studies, the engineering of crystal planes of semiconductors has become an important strategy for improving the performance of photocatalysts by fine-tuning the properties of materials. The arrangement and coordination of surface atoms essentially determine the adsorption, desorption, and carrier transfer

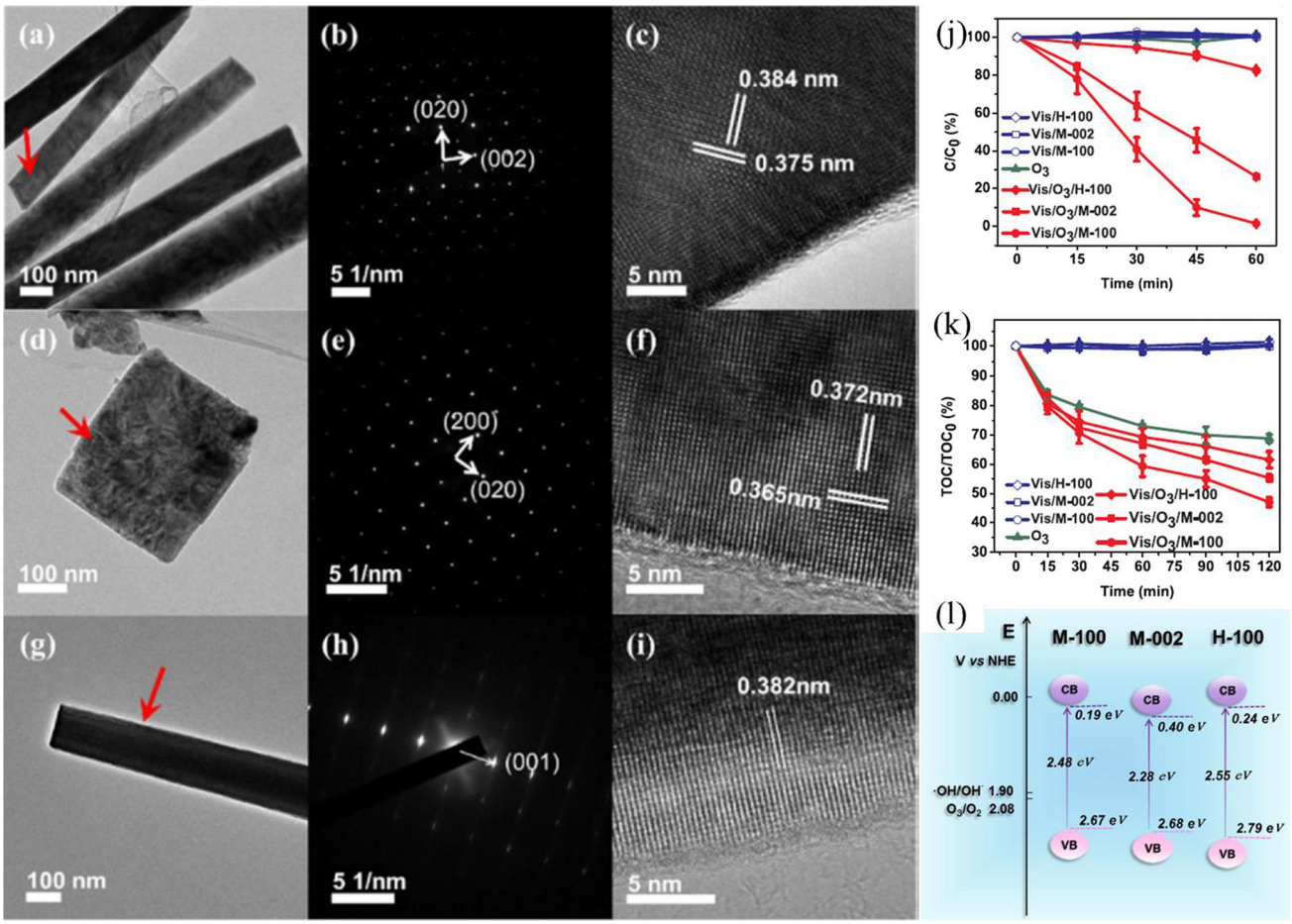

Figure 6 FETEM images of M-100 (**a**), M-002 (**d**) and H-100 (**g**). SAED images of M-100 (**b**), M-002 (**e**) and H-100 (**h**). HRTEM images of M-100 (**c**), M-002 (**f**) and H-100 (**i**). Degradation of OA (**j**) and mineralization of cephalexin (**k**) in photocatalysis, ozonation and photocatalytic ozonation; and band structures of the prepared M-100, M-002 and H-100 (**l**) (adapted with permission from reference [45], Copyright (2018) Elsevier).

efficiency of the pollutants from the surface to the adsorbed molecules. As a result, the atomic structure on the surface of the photocatalyst has a great effect on the degradation of pollutants. The atomic arrangement and coordination on the catalyst surface change with the crystal plane changing in different directions [44]. From this, we can conclude that the crystal has a great influence on the photocatalyst. In the recent years, some scholars have synthesized WO_3 materials with different crystal planes and studied their properties to compare the different crystals planes on the photocatalytic performance of WO_3.

For example, Yang et al. synthesized three different WO_3 materials and studied the degradation performance of sewage under ozone, namely monoclinic WO_3 mainly exposed to {100}, {002} monoclinic WO_3 and hexagonal WO_3 mainly exposed to {100} surface, which is called M-100 (Fig. 6a–c), M-002 (Fig. 6d–f), H-100 (Fig. 6g–i) [45]. In general, a larger surface area is beneficial for photocatalytic processes. However, in this report, M-100 has a relatively low surface area, but it owns the highest catalytic degradation performance (Fig. 6j–k), which means that the high-surface-energy facets would influence the photocatalytic performance of the photocatalysts greatly. Because M-100 has the highest CB position, it is thermodynamically conducive to the electron capture of dissolved O_3. Additionally, this study also shows that monoclinic crystals with the same crystal plane are more active than hexagonal crystals. For the same crystal, the {100} crystal plane can change the position

of the CB, compared to the {002} crystal plane, leading to the enhancement of degradation activity. Similarly, in another report, the authors also showed that the electronic structure effect of the crystal face was caused by the different atomic structure configurations on the {002}, {020} and {200} planes, which lead to the shift of the CB position (Fig. 6l) [18]. In summary, the engineering of the crystal facet is to cause the CB edge to shift upwards and then optimize the degradation activity of WO_3 on pollutants.

Some scholars have also compared WO_3 with different crystal phases [46]. Cubic WO_3 (c-WO_3) had strong adsorption on MB and increased with increasing temperature, reaching a maximum adsorption capacity of 35.95 mg/g. Monoclinic WO_3 (m-WO_3) had strong photocatalytic degradation of MB, and the degradation efficiency of MB was 100%, through the generation of photoinduced holes and hydroxyl (·OH) under 120 min of visible light irradiation. In future research, we can combine the changes of crystal plane and crystal phase to select the corresponding WO_3 for different water quality to achieve different treatment requirements and purposes.

WO_3-based heterojunction for wastewater treatment

In this section, we introduce the effect of changing the synthesis of heterojunctions based on WO_3 on the degradation of pollutants. Some scholars believe that the photocatalytic performance of one-component photocatalyst is still affected by the high recombination rate of photogenerated electron–hole pairs [49]. Therefore, the formation of heterojunctions by combining binary or ternary semiconductors with a suitable band-gap has been considered to be an effective strategy to improve the performance of photocatalysts because they can simultaneously expand the absorption range of light and promote charge separation [50]. Here, this section describes the application of WO_3 to wastewater treatment based on the synthesis of heterojunctions from different materials.

Preparing binary composites

Many studies have proved that synthetic heterojunction composites can reduce the photogenerated electron–hole recombination rate and improve the utilization of electrons and holes [51]. There are many reports on the synthesis of binary heterojunctions with WO_3 to enhance the photocatalytic activity on wastewater, such as WO_3/g–C_3N_4 [10, 50, 52, 53], WO_3/TiO_2 [54], WO_3/BiO_4 [55], WO_3/grapheme [9, 13, 20, 56, 57], etc. In particular, WO_3/g–C_3N_4 composites have been studied in detail by changing the formation of methods and conditions. WO_3/g–C_3N_4 composite photocatalysts with different photocatalytic mechanisms have been successfully prepared, such as traditional type-II and Z-scheme heterojunctions. So far, most researches on forming heterojunction composites with WO_3-based have been carried out in *p–n* heterojunctions, conventional heterojunctions, direct Z-scheme heterojunctions, and S-scheme heterojunctions. In addition to the above heterostructures, there are some special heterojunctions formed by the combination of graphene and semiconductors. The systematic improvement effect of the above mechanisms will be described below.

The *p–n* heterojunction is composed of *n*-type WO_3 semiconductors and *p*-type semiconductor [58, 59]. In the *p–n*-type heterostructure, a WO_3/BiOI heterojunction photocatalyst is taken as an example. Luo et al. proposed the photocatalytic mechanism of the WO_3/BiOI heterojunction catalyst, as shown in Fig. 7 [60]. BiOI is a *p*-type semiconductor with Fermi level (E_{f-p}) near VB, while WO_3 is an *n*-type semiconductor with Fermi level (E_{f-p}) near CB (Fig. 7a). After the *p–n*-type WO_3/BiOI heterojunction is formed, electrons will be transferred from WO_3 to BiOI, while holes will be transferred from BiOI to WO_3. When the Fermi levels of the two reached equilibrium, the internal electric field was established at the interface due to the transfer of electrons. The internal electric field can also greatly promote the migration of photogenerated carriers and effectively reduce the recombination rate of photogenerated electron–hole pairs, thereby improving the performance of photocatalyst. As shown in Fig. 7b, the Fermi level (E_{f-p}) of BiOI moves upward along the interface, and the Fermi level (E_{f-n}) of WO_3 moves upward along the interface so the migration of charge causes adjacent energy bands to occur bending. It can be found that the *p–n* structure greatly inhibits and slows down the recombination of photogenerated electrons and holes with the migration of charges and holes and the internal electric field, which can improve the photodegradation.

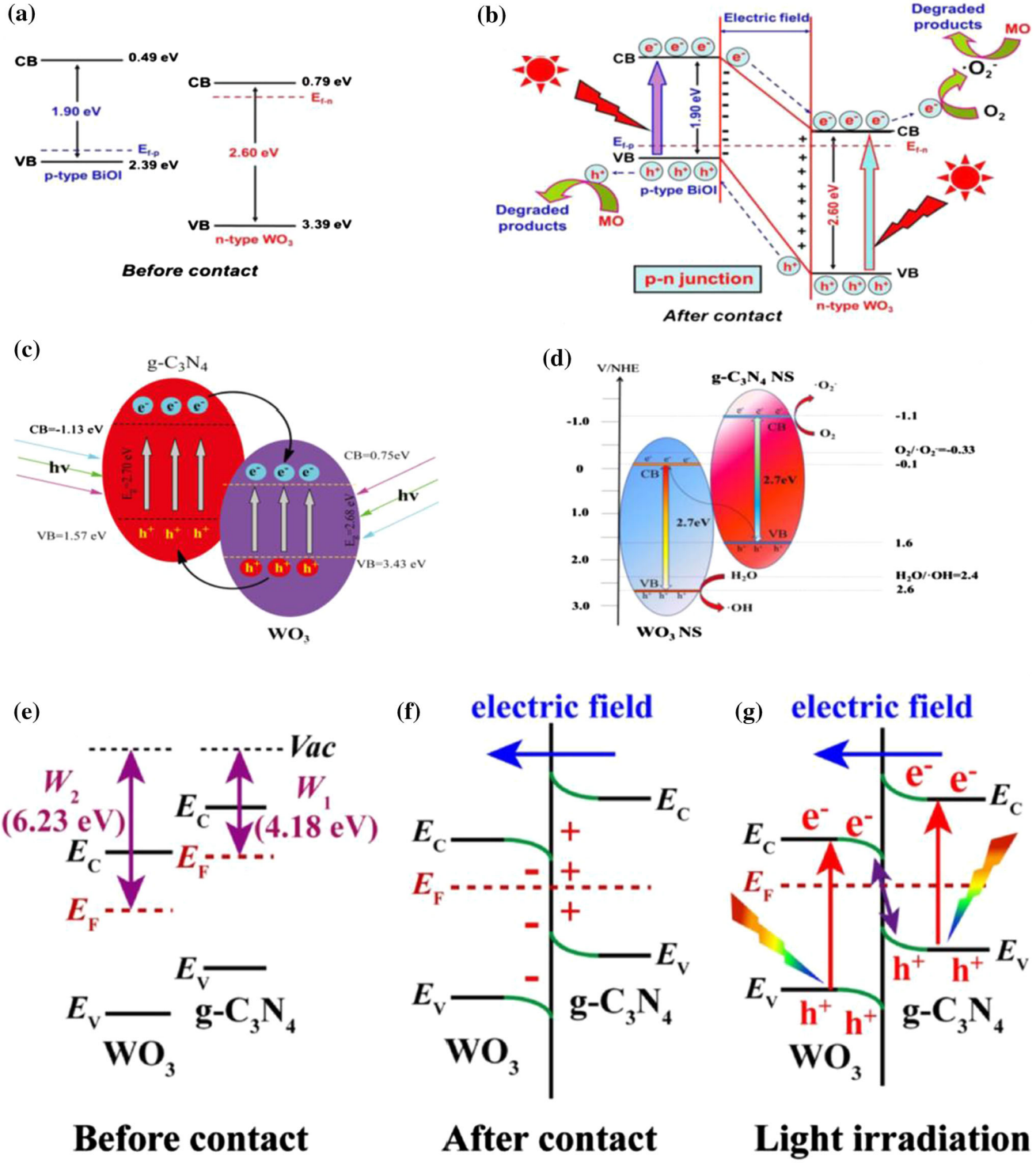
(a)
CB
0.49 eV
1.90 eV
VB
2.39 eV
p-type BiOI
CB
0.79 eV
E_{f-n}
2.60 eV
VB
3.39 eV
n-type WO_3
Before contact
(b)
Electric field
Degraded products
MO
$\cdot O_2^-$
O_2
CB
VB
p-type BiOI
1.90 eV
2.60 eV
p-n junction
n-type WO_3
After contact
(c)
g-C_3N_4
CB=-1.13 eV
hv
VB=1.57 eV
CB=0.75eV
VB=3.43 eV
WO_3
(d)
V/NHE
g-C_3N_4 NS
-1.0
0
1.0
2.0
3.0
2.7eV
-1.1
$O_2/\cdot O_2^-$=-0.33
-0.1
1.6
$H_2O/\cdot OH$=2.4
2.6
WO_3 NS
(e)
Vac
W_2
(6.23 eV)
W_1
(4.18 eV)
E_C
E_F
E_V
g-C_3N_4
WO_3
Before contact
(f)
electric field
After contact
(g)
electric field
Light irradiation

◀**Figure 7** **a** Schematic diagrams for energy bands of *p*-type BiOI and *n*-type WO_3 before contact. **b** The formation of a *p*–*n* junction and its energy band diagram at equilibrium and transfer of photoinduced electrons from *p*-type BiOI to *n*-type WO_3 under visible-light irradiation (adapted with permission from reference [60], Copyright (2015) Elsevier). **c** Proposed mechanism for the photodegradation of MB on WO_3/g-C_3N_4 composites (adapted with permission from reference [52], Copyright (2015) The Royal Society of Chemistry). **d** Schematic diagram of Z-scheme photocatalytic mechanism of WO_3 NS/g-C_3N_4 NS composite photocatalyst (adapted with permission from reference [10], Copyright (2019) Springer). **e** The work functions of g–C_3N_4 and WO_3 before contact. **f** The internal electric field and band edge bending at the interface of WO_3/g–C_3N_4 after contact. **g** The S-scheme charge transfer mechanism between WO_3 and g–C_3N_4 under light irradiation (adapted with permission from reference [63], Copyright (2019) Elsevier).

When two *n*-type semiconductors synthesize a heterojunction photocatalyst, and the two semiconductors have suitable energy bands. This mechanism is called the traditional type-II, where the electrons and holes generated by the semiconductor are transferred to the CB of semiconductor I and the VB of semiconductor II, and no electric field is generated inside. Currently reported WO_3/g–C_3N_4 heterojunctions, WO_3/$BiVO_4$ heterojunctions [55], WO_3/Ag_3VO_4 heterojunctions [59] and so on are all traditional type-II. In this type, we take WO_3/g–C_3N_4 heterojunction photocatalyst as an example. Huang and his partners synthesized a WO_3/g–C_3N_4 heterojunction through a simple calcination process in 2013 to degrade pollutants under visible light [52]. Figure 7c shows the mechanism of the WO_3/g–C_3N_4 heterojunction. Since the potential of CB and VB of WO_3 is higher than the potential of CB and VB of g–C_3N_4, the electrons generated on g–C_3N_4 are transferred to the CB of WO_3, and the photogenerated holes on VB of WO_3 are transferred to VB of g–C_3N_4. The formed electrons gather on the side of WO_3, and the holes gather on the side of g–C_3N_4, which can reduce the electron–hole recombination, thereby promoting the photocatalytic degradation of MB by the material. This mechanism is similar to the *p*–*n*-type heterojunction, but no electric field is generated. Therefore, the WO_3/g–C_3N_4 heterojunction showed higher photocatalytic degradation performance when compared to single component of pure WO_3 and g–C_3N_4 photocatalysts.

The traditional type-II heterojunction can improve the catalytic performance of the catalyst to a certain extent, but the reducibility of photo-generated electrons and the oxidizability of photo-generated holes will be reduced as the charge transfer between the semiconductors. If the semiconductor A and B are closely combined to form a heterojunction, which generates an intermediate electric field, so the heterojunction is called a Z-scheme heterojunction. This mechanism can significantly increase the space between electrons and holes, and retain its ability to redox [61]. Deng et al. successfully synthesized nanocomposite of Z-scheme WO_3 nanosheet/g–C_3N_4 nanosheet by calcination methods, and studied its photocatalytic performance [10]. Results showed that in the WO_3 NS/g–C_3N_4 NS composites with 20 wt% WO_3 NS present best photocatalytic performance, and the main reason for the improvement of degradation performance is the participation of $\cdot O^-_2$, ·OH, and h^+ in the reaction. Figure 7d shows the catalytic mechanism of Z-scheme WO_3 NS/g–C_3N_4 NS composite photocatalyst, with photogenerated electrons migrating from WO_3 NS to g–C_3N_4 NS, and photogenerated holes migrating to WO_3 NS. Therefore, a reduction reaction occurs on g–C_3N_4 with a higher reduction potential to generate $\cdot O^-_2$, and an oxidation reaction occurs in WO_3 with a higher oxidation potential to generate ·OH. The production of free radicals $\cdot O^-_2$ and ·OH optimizes the oxidation ability and the transmission efficiency of photogenerated electrons of Z-scheme WO_3 NS/g–C_3N_4 NS. At present, various forms of WO_3 and g–C_3N_4 have been successfully synthesized to form Z-scheme heterojunction photocatalysts, such as WO_3 nanorods/g–C_3N_4 nanosheets [62], WO_3 nanosheets/g–C_3N_4 nanosheet composites [10]. These complexes differently improved the photocatalytic activity of WO_3/g–C_3N_4 in the degradation of water pollutants.

Based on *p*–*n* heterojunctions, conventional type II heterojunctions, and Z-scheme heterojunctions, related scholars have proposed a new concept of stepped (S-scheme) heterojunctions [64, 65]. The S-scheme heterojunction photocatalyst consists of *n*-type oxidation photocatalysts and *n*-type reduction photocatalysts. After the equilibrium is reached, the Fermi levels of the two semiconductors are at the same level, while the photogenerated electrons will be transferred to the oxidation photocatalysts and holes will be transferred to the reduction photocatalysts, and an internal electric field will be generated.

Unlike other heterojunctions, as the S-scheme heterojunction, the electrons of CB in the oxidized photocatalytic with relatively useless and holes of VB in the reduced photocatalyst with relatively useless will recombine under the action of the internal electric field and eliminate, thereby retaining useful electrons and holes. Some scholars believe that the charge transfer path of the S-scheme heterojunction is similar to the "step" type, which has a strong redox capacity of space separation and photo-generated charge carriers [66]. Due to its unique structure and internal electric field, the S-scheme heterojunction can generate a large number of active materials to enhance the degradation efficiency of pollutants. In 2019, Fu et al. constructed a composite photocatalyst of S-scheme 2D/2D WO_3/g–C_3N_4 heterojunction through electrostatic self-assembly methods [63]. Figure 7e-g shows the mechanism of the S-scheme WO_3/g–C_3N_4 heterojunction. Generally, g–C_3N_4 is a reduction type photocatalyst with a small work function (4.18 eV) and a higher Fermi level. In contrast, WO_3 is an oxidation-type photocatalyst with a large work function (6.23 eV) and a lower Fermi level (Fig. 6e). When g–C_3N_4 and WO_3 are in close contact until the Fermi level is the same (Fig. 6f), g–C_3N_4 loses electrons and becomes positively charged, while WO_3 gets electrons and becomes negatively charged at the interface. As a result, an internal electric field is generated at the interface and the band edges are bent of the two semiconductors, which can make some electrons from WO_3 CB combine with holes from g–C_3N_4 VB. But this way can prevent electrons from g–C_3N_4 CB from combining with holes from WO_3 VB, shown in Fig. 6g. In general, this heterojunction mechanism can recombine the relatively useless electrons and holes in the two semiconductors, while the useful electrons and holes are retained. It is because of this unique transfer process of electrons and holes that the 2D/2D WO_3/g–C_3N_4 composites have strong oxidation and reduction ability, thereby improving the photocatalytic performance of composites. The mechanism has been shown to exhibit strong photocatalytic activity against water decomposition. Unfortunately, no research has been done on S-scheme WO_3-based binary composite heterojunctions for wastewater. However, this mechanism shows great potential in terms of photocatalysis, and this photocatalytic mechanism will show greater potential in water pollution treatment in the future.

Within ordinary heterojunctions, Z-scheme and S-scheme heterojunctions, there are special heterojunctions formed by the combination of graphene (GR) and semiconductors. Graphene is a two-dimensional single-layer SP^2 hybrid carbon atom with excellent charge transfer performance, high thermal conductivity, high surface area and hexagonal filled structure [67]. The ultra-high electrical conductivity and low conduction band potential (-0.08 V vs. SHE, pH = 0) of graphene allow photo-generated electrons to flow from the semiconductor to its surface, thereby reducing the compound photo-generated electrons-holes. In 2010, Zhang et al. first proposed the application of graphene in photocatalysis and they proved that the addition of graphene improved the degradation efficiency of MB in the composites [68]. Based on graphene, people also synthesize GO and RGO to synthesize composite materials with semiconductors. So far, many scholars have successfully prepared composite photocatalysts composed of WO_3 and graphene with different morphological structures, such as WO_3 nanoparticles [69], one-dimensional nanostructures [20, 70], two-dimensional nanosheets [13, 71] and so on, and all have proved the synthesized composites materials can significantly enhance the ability to degrade water pollution. Guo et al. synthesized WO_3 nanoparticles on the graphene sheets by the sonochemical method [72]. Studies have shown that the amount of O_2 precipitated from the water of WO_3@GR composites with 40 wt% GR inside was twice that of pure WO_3. The improvement in photocatalyst performance was the result of the joint action of WO_3 nanoparticles and GR sheets, through enlarging the absorption range of visible light, enhancing the electron transport and promoting the separation of photogenerated charge carriers. The mechanism diagram is shown in Fig. 8a. As we all know, the application of one-dimensional single-crystal nanomaterials in photocatalysis is very important. Compared with nanoparticles, one-dimensional materials have smaller grain boundaries, which provide the path for photo-generated charges and inhibit free electron scattering, thereby having higher photocatalytic activity. For example, in 2012, An et al. synthesized WO_3 nanorods on the surface of graphene through the hydrothermal method, and the mechanism shown in Fig. 8b [20]. Studies have shown that the degradation efficiency of rhodamine B 6G (RhB 6G) by WO_3/graphene composites containing 3.5wt% graphene was 2.2 times than that of pure

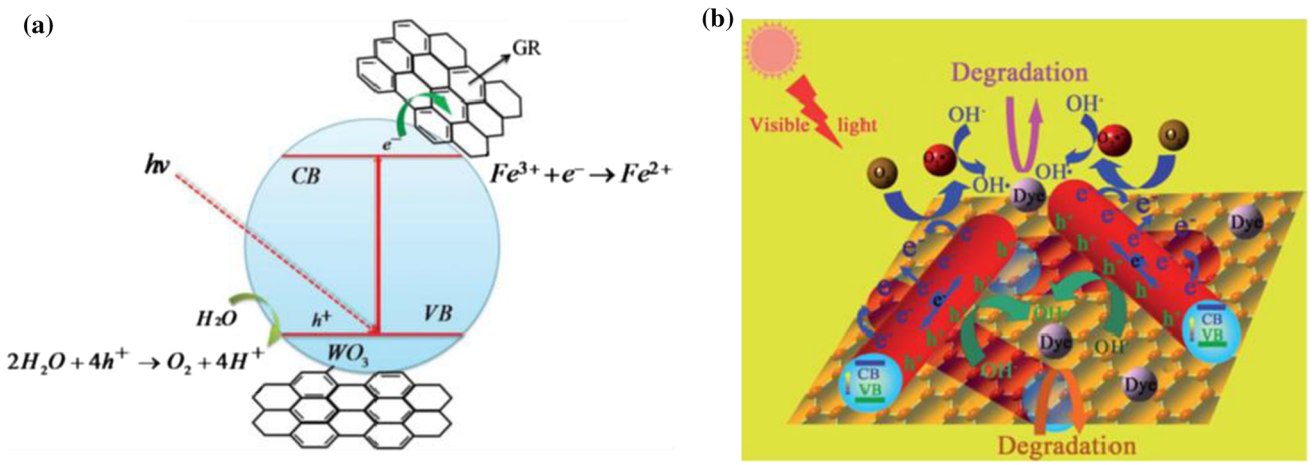

Figure 8 **a** The procedure of photocatalytic oxidation for the WO_3@GR composite (adapted with permission from reference [72], Copyright (2012) The Royal Society of Chemistry). **b** Proposed photodegradation mechanism of RhB 6G over WO_3 nanorods/graphene composites (adapted with permission from reference [20], Copyright (2012) The Royal Society of Chemistry).

WO_3 nanorods. They believe that the interaction between dyes and negatively charged groups in graphene can result in higher adsorption capacity of RhB 6G for WO_3/graphene and improve migration of photo-generated carriers are important factors to improve the photocatalytic performance of WO_3/graphene.

Preparing ternary composites

To date, many binary composites based on WO_3 have been synthesized. However, studies have shown that ternary nanocomposites generally have wider visible light response range, lower recombination rate and higher interfacial charge transfer than binary nanocomposites [73–76]. Among the ternary composites of WO_3-based, there are two kinds of semiconductors combined with electronic mediators to synthesis composite materials, and there are three kinds of semiconductors, which we will discuss separately.

In ternary Z-scheme heterojunctions, electron mediators are usually used as conductive materials to improve electron transfer, such as Ag [77–79], Au [80], carbon nanodots [81] and RGO [82]. Because the Fermi level of the electron mediator is between two semiconductors, the electron mediator and the two semiconductor materials form a Z-scheme photocatalytic mechanism. Here, take redox graphene (RGO) and metallic Ag nanoparticles as examples. For example, in 2018, Lu et al. successfully prepared Z-scheme WO_3/RGO/g–C_3N_4 composite materials, in which RGO is an electron mediator [83]. The degradation mechanism is shown in Fig. 9a. RGO, as an electron mediator, changes the charge transfer pathway of the composite, which is different from the binary Z-scheme heterojunction. In the ternary Z-scheme WO_3/RGO/g–C_3N_4 composite, the photo-generated electrons on CB of WO_3 combined with the holes on VB of g–C_3N_4 through RGO in the interface between RGO and g–C_3N_4. Thus, useful electrons and holes are retained for generating the radicals $\cdot O^-_2$ and ·OH. Free radicals can participate in the oxidation reaction, thereby improving the performance of WO_3/RGO/g–C_3N_4 photocatalyst. Also in 2019, Chen et al. successfully synthesized WO_3 nanoplate/Ag/g–C_3N_4 nanosheet compound materials by solvent evaporation and in situ calcination [77]. The study showed that WO_3/Ag/g–C_3N_4 can degrade RhB about 96.2% in 40 min, while the degradation efficiency of RhB by WO_3/g–C_3N_4 is 58.2% under the same conditions. The synergistic effect of g–C_3N_4 nanosheets and WO_3 nanoplates beneficial to enhance photocatalytic performance can provide conditions for the rapid transfer of photo-generated electrons and holes, and the electron mediator Ag nanoparticles are conducive to the charge transfer (Fig. 9b). Moreover, the Z-scheme heterostructure allows the composite to retain high redox capacity. Excellent photocatalytic activity, easy design and easy manufacturing are all

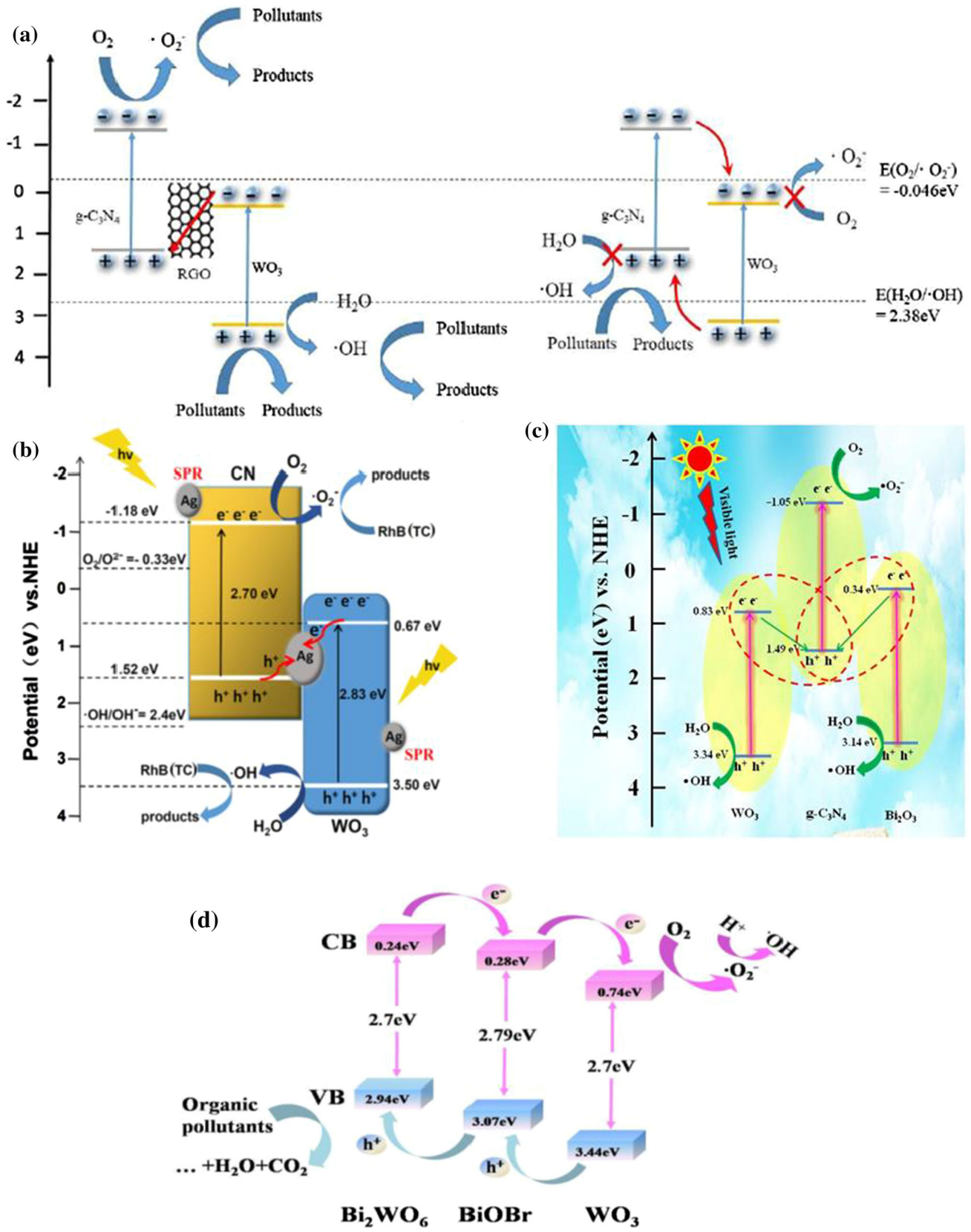
(a)
Pollutants
Products
O_2
$\cdot O_2^-$
g-C_3N_4
RGO
WO_3
H_2O
$\cdot OH$
Pollutants
Products
Pollutants
Products
$\cdot O_2^-$
$E(O_2/\cdot O_2^-)$ = -0.046eV
O_2
g-C_3N_4
H_2O
$\cdot OH$
WO_3
$E(H_2O/\cdot OH)$ = 2.38eV
Pollutants
Products
(b)
hv
SPR
CN
Ag
O_2
$\cdot O_2^-$
products
RhB(TC)
-1.18 eV
O_2/O^{2-} =- 0.33eV
2.70 eV
1.52 eV
$\cdot OH/OH^-$= 2.4eV
0.67 eV
2.83 eV
3.50 eV
SPR
RhB(TC)
$\cdot OH$
products
H_2O
WO_3
Potential (eV) vs.NHE
(c)
Visible light
O_2
$\cdot O_2^-$
-1.05 eV
0.83 eV
0.34 eV
1.49 eV
H_2O
3.34 eV
$\cdot OH$
H_2O
3.14 eV
$\cdot OH$
WO_3
g-C_3N_4
Bi_2O_3
Potential (eV) vs. NHE
(d)
CB
0.24eV
0.28eV
0.74eV
e^-
O_2
H^+
$\cdot OH$
$\cdot O_2^-$
2.7eV
2.79eV
2.7eV
VB
2.94eV
3.07eV
3.44eV
Organic pollutants
… +H_2O+CO_2
h^+
h^+
Bi_2WO_6
BiOBr
WO_3

◀**Figure 9** **a** Schematic illustration of the separation and transfer of photogenerated charges and the reactive species in the degradation process of Z-scheme photocatalyst g–C_3N_4/RGO/WO_3 (left) and heterojunction*n*-type photocatalyst g–C_3N_4/WO_3 (right) (adapted with permission from reference [83], Copyright (2018) Elsevier). **b** Photocatalytic mechanism for WO_3/Ag/CN composite under visible light irradiation (adapted with permission from reference [77], Copyright (2018) Elsevier). **c** Schematic diagram for the possible charge separation of Z-scheme WO_3/g–C_3N_4/Bi_2O_3 (adapted with permission from reference [17], Copyright (2018) Elsevier). (d) Schematic diagram for the possible charge separation of flower-like BiOBr-WO_3–Bi_2WO_6 ternary hybrid (adapted with permission from reference [88], Copyright (2015) Elsevier).

advantages of binary Z-scheme composite photocatalyst. However, the composite materials have the disadvantages, such as low surface area, small response range of visible light, poor adsorption performance, and weak redox capacity. The electron mediator usually provides a close contact area between WO_3 and other semiconductors, so that the electrons are better transferred, the photogenerated electron–hole pairs recombination is reduced, and the degradation efficiency is improved. This mechanism is similar to the S-scheme mechanism through the combination of relatively useless electrons and holes to leave useful electrons and holes, which use useful electrons and holes to generate free radicals to improve photocatalytic activity. At present, some scholars have proposed to form ternary S-scheme heterojunctions by doping electron mediators. For example, Pan et al. doped C in S-scheme 2D/2D WO_3/g–C_3N_4 and studied the photocatalytic ability to degrade MB [64]. The degradation of MB can reach 92.4% in 60 min. When C as electron mediator, the heterojunction has high redox capacity, short charge transfer distance, and wide response range of visible light, which greatly improves photocatalytic ability.

The Z-scheme composites coupled with three kinds of semiconductors can produce more electrons and holes to improve the photocatalytic performance of the composites. Recently, scholars have successfully synthesized ternary Z-scheme complexes based on WO_3, such as WO_3/MoS_2/g–C_3N_4 and WO_3/g–C_3N_4/Bi_2O_3 84] presenting much better photocatalytic abilities than binary Z-scheme photocatalytic systems. For example, Jiang and his partners have synthesized the Z-scheme WO_3/g–C_3N_4/Bi_2O_3 composite through a one-step co-calcination strategy and proved that the material has excellent photocatalytic performance [17]. The migration of electrons along the interface leads to accumulating in the CB of g–C_3N_4, while holes accumulate in the VB of WO_3 and Bi_2O_3 shown in Fig. 9c. Therefore, the electrons in the CB of g–C_3N_4 can be captured by O_2 to generate $\cdot O^-_2$, while the holes in VB of WO_3 and Bi_2O_3 can oxidatively degrade TC or oxidize H_2O to form ·OH radicals. Active free radicals then participated in the degradation of pollutants, which increased the degradation rate of TC by the composites.

In addition to ternary semiconductors coupled into Z-scheme composites, ternary semiconductors are coupled into cascade structures, in which electrons and holes migrate through the interface potential gradient in the ternary mixed-valence band. WO_3/Bi_2WO_6/BiOBr, WO_3/TiO_2/CdS, WO_3/Cu_2O/$BiVO_4$, and WO_3/$BiVO_4$/BiOCl have been reported [85–87]. For example, Zhu et al. successfully prepared flower-like WO_3-BiOBr-Bi_2WO_6 ternary composites, in 2015 [88]. The experimental results showed that the composite material showed higher photocatalytic activity compared with the WO_3-Bi_2WO_6 binary composite, and the degradation mechanism of RhB by this material is proposed (Fig. 9d). In Fig. 9d, it can be seen that the CB edge of BiOBr is located between Bi_2WO_6 and WO_3. Therefore, the ternary composite can form a cascade structure, similar to the traditional type-II heterojunction. For the WO_3-BiOBr-Bi_2WO_6 material, the electrons are accumulated in the CB of WO_3 and the holes are accumulated in Bi_2WO_6 by the migration of charge carriers. So the electrons on the surface of WO_3 and the hydroxyl radicals generated by the holes on the surface of Bi_2WO_6 can directly participate in the reaction to degrade organic pollutants. WO_3-BiOBr-Bi_2WO_6 cascade structure has improved RhB degradation efficiency by high surface area, close interfacial contact, and differences in energy band positions. Besides, the cascade CB positioning of the ternary semiconductor will generate a built-in potential gradient, which can better promote the separation of photo-generated electrons and holes, thereby promoting electron transfer within the junction structure. This conclusion has been proved in other reports [86, 87].

From this, in the process of degradation of sewage with WO_3 photocatalyst, Z-scheme ternary composites, and ternary cascade composites can enhance the

degradation of organic compounds. In the recent years, many scholars have proposed that heterojunction composites have great potential in the degradation of water pollution. Therefore, the formation of Z-scheme (or S-scheme) heterojunctions can obtain the best performance by increasing the absorption range of visible light, increasing the specific surface area, promoting effective charge separation, strengthening interface contact and generating free radicals (Table 2).

Element modification of WO_3 for wastewater treatment

At present, some scholars have used non-metal and metal to modify semiconductors for improving the photocatalytic degradation performance of WO_3 on sewage. Because the modification of elements in photocatalyst can enhance the photocatalytic activity of photocatalysts by enhancing the separation rate of photogenerated electron–hole pairs and increasing the photo-response range of visible light. So far, Fe, Ni, Cu, Zn, Co, and other metal ion-doped WO_3 composite materials and N, S, C, P, I, F and other non-metal ion-doped composite materials have been successfully synthesized. Co-doping of elements can promote the separation of photogenerated electrons and holes faster, which means that the co-doping of elements WO_3 is more conducive to the improvement of photocatalytic performance. In this section, the photocatalytic degradation properties of transition metals, precious metals, rare earth metals, non-metals, and multi-element co-doped materials are studied. The results are summarized in Table 3.

Metal element doping

Co, Zn, Ni, Cu, and Fe transition metals have been studied to dope WO_3 to widen the visible light response range of WO_3 for improving the photocatalytic activity of WO_3. Hameed and his colleagues studied the effect of Co, Zn, Ni, Cu-doped WO_3 on photocatalysis [100]. Studies have shown that among transition metals, the doping of Ni has the greatest effect on the catalytic hydrogen production of WO_3. When doped with 1.0% and 10.0% Ni, the photocatalytic oxygen generation efficiency of WO_3 was 4 times and 19 times of the original. However, oxygen production and hydrogen production are different. By doping pure WO_3 with 10% Fe, WO_3 had the highest hydrogen production capacity, in which the hydrogen production was 7 times that of the original. The effect of doping different concentrations of Fe on the degradation of RhB by WO_3 was also reported [101]. When Fe was doped at 5.25%, WO_3 had the highest photocatalytic efficiency under visible light. About 93% of phenol was reduced in 240 min, and about 92% of RhB was degraded in 120 min by 5.25% Fe-doped WO_3. When 5% Fe-doped WO_3 showed the best photocatalytic performance in MB degradation, it could degrade about 95% of MB in 120 min under visible light irradiation [102]. Thereby, the transition metal-doped WO_3 shows higher photocatalytic degradation ability when treating organic compounds in wastewater.

The rare earth metals in the periodic table include 17 elements, which can be used as dopants for WO_3 semiconductors to degrade organic pollutants. In the recent years, some scholars have proposed that doping rare earth metals into WO_3 can promote the concept of charge separation. Because the 4f orbit of the rare earth metal is not completely occupied, and the 5d orbit is empty, it can effectively capture electrons, which can effectively promote the separation of the photogenerated carrier, thereby playing an important role in doping for improving the performance of photocatalysis [103]. The effects of doping rare earth metals such as Gd 104], Dy [105], La [106], Eu [107], and Yb [108] on the photo-activity and photo-stability of WO_3 have been studied. In the case of Dy-WO_3, Dy^{3+} can provide electrons to the adsorbed oxygen and then convert it to Dy^{4+}, thereby promoting the generation of superoxide radicals. Besides, Dy^{4+} can trap electrons in WO_3 CB and inhibit photo-generated electron–hole recombination. WO_3 may be partially consumed in aqueous solution, and Dy^{3+} doping will hinder this deactivation process [109]. Tahi et al. used a hydrothermal method to synthesize rare metal-modified WO_3 composites [104]. Studies have shown that the doping of rare metals affects the grain size and specific surface area of the photocatalyst so that WO_3 exhibits excellent photocatalytic performance during the degradation of harmful dyes. Among them, doping 2% Gd showed the most effective degradation performance of WO_3, and the degradation efficiency of various pollutants could reach about 98%. Although doped rare earth metals are very expensive, they have great potential for improving the WO_3 degradation of pollutants.

Table 2 Modification for enhancing the photocatalytic activity by using WO_3-based photocatalyst

Photocatalyst		Pollutant	Concentration of pollutant	Method	Light source	Mass ratio	Results	Ref
Binary composites								
p–n	WO_3/BiOI	MO	10 ppm	Hydrothermal method	500 W Xe-arc lamp ($\lambda > 420$ nm)	WO_3:BiOI = 1:99	67% in 100 min	[60]
	WO_3/Ag_2CO_3	RhB	30 ppm	Hydrothermal method	350 W Xe lamp	WO_3:Ag_2CO_3 = 4:1	99% in 18 min	[59]
Traditional type-II	WO_3/g-C_3N_4	MB	10 ppm	Calcination method	300 W Xe lamp at 400 nm	WO_3:g-C_3N_4 = 1:9.41	97% in 120 min	[52]
	WO_3/Ag_3VO_4	TC	10 ppm	Hydrothermal method and precipitation method	300 W Xe lamp ($\lambda > 420$ nm)	WO_3:Ag_3VO_4 = 1:9	71.2% in 30 min	[89]
	WO_3/Bi_2MoO_6	RhB	20 ppm	Electrospinning–calcination–solvothermal method	300 W Xe lamp ($\lambda > 400$ nm)	WO_3:Bi_2MoO_6 = 1:6.58	100% in 90 min	[90]
	WO_3/$BiFeWO_6$	RhB	47.9 ppm	Co-precipitation and hydrothermal methods	250 W tungsten halogen lamps	WO_3:$BiFeWO_6$ = 99:1	83% in 60 min	[91]
Z-scheme	WO_3/g-C_3N_4	MB	3.35 ppm	Ball milling and heat treatment methods	500 W Xe lamp at 400–470 nm	WO_3:g-C_3N_4 = 1:19	87.9% in 60 min	[92]
		BF	3.65 ppm				75.6% in 60 min	
	WO_3 NS/ g-C_3N_4 NP	RB5	20 ppm	Ultrasonic method	solar light irradiation	WO_3:g-C_3N_4 = 1:3	93% in 90 min	[93]
		RhB	10 ppm	Solvent evaporation and in situ calcination method	XG500 Xe long-arc lamp ($\lambda > 420$ nm)	WO_3:g-C_3N_4 = 1:5	58.2% in 40 min	[77]
	WO_3 NS/ g-C_3N_4 NS	RhB	14.37 ppm	Calcination method	1000 W Xe lamp	WO_3:g-C_3N_4 = 1:4	78.6% in 100 min	[10]
		MO	10 ppm	Direct precipitation method	LED-light illumination at 410 nm	WO_3:g-C_3N_4 = 1.85:1	96.8% in 120 min	[53]
	WO_3/Ag_3PO_4	TC	20 ppm	Surfactant-free hydrothermal method	300 W Xe lamp ($\lambda > 420$ nm)	WO_3:Ag_3PO_4 = 1:1	96% in 20 min	[94]
		MB	20 ppm	Hydrothermal method	300 W Xe lamp($\lambda > 420$ nm)	WO_3:Ag_3PO_4 = 1:1.8	95% in 60 min	[95]
		MO	20 ppm				90% in 180 min	
	WO_3@SnS_2	RhB	20 ppm	Two-step hydrothermal method	5 W white light LED	WO_3:SnS_2 = 11.76:1	94.1% 100 min	[96]
	WO_3/ $HTiNbO_5$ NS	RhB	10 ppm	Hydrothermal method	300 W Xe lamp	WO_3:$HTiNbO_5$ = 1:9	≈90% 100 min	[97]

Table 2 continued

Photocatalyst		Pollutant	Concentration of pollutant	Method	Light source	Mass ratio	Results	Ref
WO_3/graphene	WO_3/GR	MB	10 ppm	Hydrothermal method	500 W tungsten halogen lamp	WO_3:GR = 93:7	94% in 8 h	[70]
	WO_3/GO	MB	20 ppm	Ultrasonication method	sunlight	WO_3:GO = 1:3	97.03% in 180 min	[57]
		IC	20 ppm				95.43% in 120 min	
	WO_3/RGO	p-cresol	20 ppm	Hydrothermal method	250 W lamp	WXO_3:rGO = 30:1	57.3% in 6 h	[56]
		Cr(VI)	20 ppm				95.2% in 6 h	
	WO_3 NP/RGO	SMX	20 ppm	Step hydrothermal method	200 W Xe arc lamp at 420-630 nm	WO_3:RGO = 40:1	98% in 180 min	[71]
Ternary composites								
Z-scheme	WO_3/Ag/Ag_2CO_3	RhB	20 ppm	Facile deposition and photochemical reduction method	300 W Xe lamp($\lambda > 420$ nm)	20wt% WO_3	99.13% in 60 min	[78]
		MO	10 ppm				96.15% in 90 min	
	WO_3/Ag/g-C_3N_4	RhB	10 ppm	Solvent evaporation and in situ calcination method	XG500 Xe long-arc lamp ($\lambda > 420$ nm)	WO_3:Ag:g-C_3N_4 = 3.7:1:18.5	96.2% in 40 min	[77]
	WO_3/GO/Fe_2O_3	MB	20 ppm	–	300 W solar simulator	WO_3:GO:Fe_2O_3 = 4.8:1:3.3	95% in 60 min	[98]
		CV	20 ppm	–			95% in 60 min	
	WO_3/rGO/$SnIn_4S_8$	Cr(VI)	–	Combined protocol of the in situ precipitation method with hydrothermal method	300 W Xe lamp ($\lambda > 420$ nm)	WO_3:RGO:$SnIn_4S_8$ = 4:1:20	93.5% in 30 min	[99]
		RhB	–			WO_3:RGO:$SnIn_4S_8$ = 2:1:20	100% in 60 min	
	WO_3/MoS_2/g-C_3N_4	RhB	50 ppm	Co-calcination, hydrothermal method	300 W Xe arc lamp($\lambda > 420$ nm)	–	99% in 10 min	[84]
		MB	20 ppm				83.4% in 60 min	
		MO	20 ppm				91.8% in 60 min	
		AO_7	20 ppm				94.2% in 60 min	
	WO_3/g-C3N_4/Bi_2O_3	TC	10 ppm	Co-calcination method	300 W Xe lamp($\lambda > 420$ nm)	–	80.2% in 60 min	[17]
S-scheme	WO_3/C/g-C_3N_4	TC	20 ppm	One step co-calcination method	300 W Xe lamp($\lambda > 420$ nm)	–	90.54% in 60 min	[64]
Cascade structures	WO_3/$BiVO_4$/BiOCl	RhB	10 ppm	Two-step synthetic method	300 W Xe lamp	–	69.5% in 180 min	[85]
	WO_3/Bi_2WO_6/BiOBr	RhB	10 ppm	Effective two-step method	500 W Xe lamp($\lambda > 420$ nm)	WO_3:Bi_2WO_6:BiOBr = 1:2.6:15	98% in 90 mix2n	[88]

Table 3 Element modification for enhancing the photocatalytic activity of WO_3 photocatalyst

Photocatalyst	Pollutant	Method	Light source	Optimum doping	Results	Ref
Transition metal doping						
Co-WO_3 nanoplates	Methyl red	Chemical co-precipitation method	500 W lamp ($\lambda > 400$ nm)	5%	90% in 120 min	[126]
Ni-WO_3 nanoplates	Methyl red	Chemical co-precipitation method	visible light	5%	96% in 120 min	[127]
Fe-WO_3	Phenol RhB	Template method	300 W Xe lamp	5.25%	93% in 240 min 92% in 120 min	[101]
Ir-WO_3	MB CV	Single step hydrothermal method	Visible light	3%	97% in 60 min 99% in 60 min	[128]
Rare earth metals doping						
Gd-WO_3	MB	Hydrothermal method	400 W metal halide lamp($\lambda \geq 400$ nm)	2%	98% in 90 min	[104]
La-WO_3 NPs	RhB	Crystallization precipitation method	1000 W Xe lamp ($\lambda > 400$ nm)	2.4 mmol	≈90% in 10 h	[106]
Dy-WO_3 NPs	RhB	Precipitation method	250 W Hg lamp at 290–450 nm	0.25 M	91.2% in 180 min	[105]
Eu-WO_3 NPs	RhB	Pechini's method	UV	–	≈100% in 60 min	[107]
Yb-WO_3	MO	Pray pyrolysis technique	UV lamp at 365 nm	3 at%	96% in 320 min	[108]
Non-Metal doping						
S-WO_3	MB	Hydrothermal method	300 W Xe lamp	5%	78.7% 2.5 h	[110]
S-WO_3 nanowires	MO	Hydrothermal method	visible light at 420 nm	3%	Remove 97% in 3 h	[112]
N-WO_3	MO	Annealing anodic oxide layers	500 W Xe lamp ($\lambda \geq 400$ nm)	–	Remove 25% in 60 min	[113]
C-WO_{3-x} ultrathin nanosheets	N-t-butylbenzylamine	Acid-assisted one-pot method	500 W Xe lamp ($\lambda > 400$ nm)	D	Oxidation 50% in 14 h	[114]
I-WO_3	local dyeing wastewater	One-step green synthesis of WO_3 based on the interaction of ammonium para tungstate and Spondias mombin leaves extract	natural sunlight	–	88.19% and 89.14% for TOC and COD reduction in 240 min	[118]
P-WO_3					86.8% and 86.63% for TOC and COD reduction in 240 min	

Table 3 continued

Photocatalyst	Pollutant	Method	Light source	Optimum doping	Results	Ref
Co-doping						
I-P-WO_3	local dyeing wastewater	One-step green synthesis of WO_3 based on the interaction of ammonium para tungstate and Spondias mombin leaves extract	natural sunlight	2%	93.40% and 95.14% for TOC and COD reduction in 240 min	[70]
DD	gentamicin antibiotic	Precipitation and co-precipitation methods	125 W UV lamp at 365 nm	/D	≈90% in 90 min	[77]
Noble metal deposited						
Pt-WO_3	2,4-Dichlorophenoxyacetic acid	Photochemical impregnation method	230 W tungsten-halogen lamp at 230 nm	1%	80% in 30 min	[124]
Pt-WO_3	MB	The sol–gel method	250 W visible lamp at 400–700 nm	0.5 wt.%	90% in 70 min	[129]
Pd-WO_3	E. coli microorganism from water	Impregnation method	UV laser radiation at 355 nm	10wt%	100% eliminated in 8 min	[119]
Ag-WO_3 nanoplates	SAM	Hydrothermal method and photo-reduction method	200 W Xe arc lamp at 420–630 nm		96.2% in 5 h and 100% removal Escherichia Coli and Bacillus subtilis in 2 h	[125]

Non-metal element doping

The above-mentioned that the performance of the catalyst can be enhanced through doping metals, but some researchers have found that metal-doped semiconductors are not heat-resistant and may cause photoelectron-hole pair recombination [110]. Therefore, it is proposed that doping non-metals can also improve the wide band-gap and promote the separation of photogenerated carriers [111]. Some researchers have demonstrated that doping non-metals can enhance the performance of WO_3 photocatalyst [110, 112–114]. For example, Chen et al. synthesized S-doped WO_3 samples by the hydrothermal method [110]. Experimental results showed that compared with undoped WO_3, S-WO_3 samples had better photo-degradability, and the maximum MB removal efficiency of 5% S-WO_3 samples was 78.7%. It is attributed to the lower bandgap energy, more oxygen vacancies in the surface lattice and the heterojunction formed by WS_2 and WO_3. Because the CB position of WS_2 was higher than the CB position of WO_3, which caused the generated electrons to be injected into the CB of WO_3, resulting in effective charge separation. Therefore, non-metal-doped WO_3 shows higher photocatalytic degradation ability than undoped WO_3 when treating organic compounds in wastewater treatment.

Elements co-doping

In addition to single-element doping, multi-element co-doping has also been used to increase the efficiency of WO_3 photocatalysts [115]. Multi-element co-doped WO_3 composites have been successfully synthesized and proved to have good photocatalytic properties, such as Zn-Cu co-doped WO_3 [116], Nb-F co-doped WO_3 [117], and so on. Here, we take I-P co-doped WO_3 as an example. Tijani et al. prepared the I-P elements co-doped WO_3 nanoparticles and studied the photocatalytic performance of the material to degrade the local wastewater contaminated with dyes [118]. The found that spherical WO_3 nanoparticles can be completely transformed into rods and bamboo bundles with different doping percent of I and P elements, and the relative images are shown in Fig. 10. For I-P co-doped WO_3, it can be observed that the relative morphology can be transferred from spherical symmetry into rod-like structure by adjusting the doping content of different I and P element. The reasons may refer to the fact that the nature of the dopant vis-a-vis atomic weight and ionic size can make great influence on the morphology of the target materials. Compared with the undoped WO_3 with spherical and cubic structure, both I^- and P^{+3} dopants can be treated as the structure directing agents for the formation of a less compacted rod and hexagonal nanostructures. The detail morphology adjustment mechanism can be explained as follows: the formation of the nanorods liked WO_3 with 10% iodine or phosphorus mainly originated from the side-by-side alignment, which caused by the high lateral capillary forces; the formation of bamboo-like or nanorods bundles liked I-P co-doped WO_3 refers to the oriented attachment, which caused by the reduction of the surface energy due to the synergetic effect between I and P element [118]. As for the photocatalytic performance, I-P co-doped WO_3 nanocomposites can degrade 93.4% TOC and 95.14% COD, and show the highest photocatalytic activity compared with single-doped and undoped WO_3. I^- and P^{+3} occupied the oxygen vacancies in WO_3 nanoparticles, but through the synergy between the two dopants, the crystal size was reduced and the surface area was increased. As a result, some I and P diffused on the surface of WO_3, which may cause surface defects, thereby improving the degradation of printing and dyeing wastewater. Also, local internal electric field determined by both I and P can make the rapid separation of photogenerated carriers to improve the degradation efficiency. In general, this material had many advantages, such as higher specific surface area, smaller band-gap energy, good crystallinity, wider visible light response range, and lower photo-generated electron–hole recombination rate. It can be obtained that the presence of co-dopants can further improve the photocatalytic degradation ability of WO_3 doped with a single element on wastewater.

Deposition of noble metal

At present, the research on the deposit of WO_3, such as Au, Pt, Ag, Pd and so on, shows that the degradation performance of WO_3 can be improved by improving charge transfer, increasing electron traps and reducing band-gap energy. It has been reported that noble metal-deposited WO_3 nanoparticles improve photocatalytic activity by adjusting the Fermi level balance between noble metal and WO_3

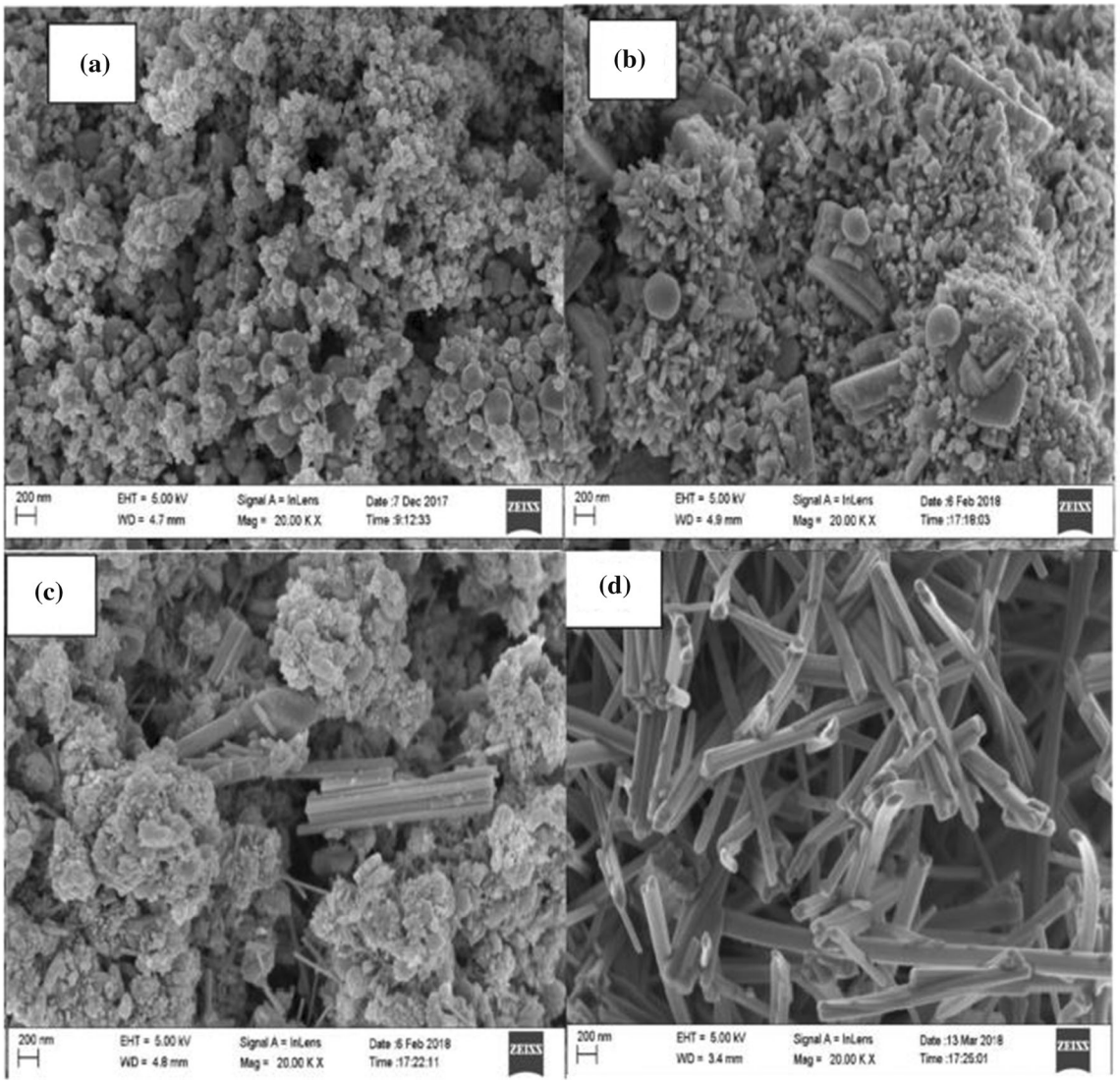

Figure 10 HR-SEM images for **a** undoped WO_3, **b** 2% I-doped WO_3, **c** 2% P-doped WO_3 and **d** 2% P and I co-doped WO_3 (adapted with permission from reference [118], Copyright (2019) Elsevier).

photocatalyst to reduce band-gap energy [119], and suppress electron–hole recombination [120]. As early as 2010, scholars reported that the deposition of Pt can improve the performance of WO_3 photocatalyst [121]. The effect of WO_3 with different shapes of Pt deposited on ethylene under visible light was also studied. Studies have shown that the order of photoactivity is Pt/nanocubes > Pt/nanoparticles > Pt/nanobundles [122]. WO_3 nanocube had the best photo-degradability due to its unique geometry. The presence of Pt deposits improved the photo-activity of nanoparticles and nanocubes, which was attributed to the ability of Pt deposits to promote the multi-electron reduction of O_2. Also, some scholars have compared the photocatalytic performance of Pt loaded with different shapes of WO_3 [123]. According to the photocatalytic evaluation results of Pt-loaded samples, the sequence of the most active sample was not significantly different from that of the unloaded sample. This meant that the morphological structure of WO_3 on the photocatalytic degradation ability was greater than that of the supported co-catalyst. At the same time, the size of noble metal particles also affects the performance of WO_3. The deposition of Au nanoparticles was not conducive to improving the activity of WO_3 to degrade pollutants. Because the

size of Au nanoparticles was too large, and most of the surface of WO_3 was covered by gold particles, which prevented the incident light from reaching the surface and made this part of the catalyst in an inactive state during the reaction [124]. The effect of different concentrations of deposited Ag on the degradation efficiency of sulfanilamide (SAM) was also studied [125]. Within a certain range, the degradation efficiency increased with the increase in Ag concentration. Ag nanoparticles as electron capture centers during WO_3 degradation SAM process can improve the separation of photogenerated electrons. Moreover, WO_3/Ag composites could also deactivate *Escherichia Coli* and *Bacillus subtilis* under visible light. The antibacterial effect can be attributed to synergistic effect among Ag, Ag^+, and antibacterial of WO_3/Ag composite. Therefore, the photocatalytic degradation ability of noble metal-deposited WO_3 is higher than that of WO_3 without noble metal deposition when treating organic compounds in wastewater. And it has great potential in treating wastewater contaminated by pathogens.

Conclusions and future prospective

Many studies have shown that WO_3 is a promising photocatalyst for water pollution treatment by responding to visible light because of its highly adjustable performance and excellent performance in removing persistent organic micro-pollutants and some microorganisms in complex water performance. Through a variety of improvement measures, scholars have synthesized WO_3-based materials with large specific surface area and charge separation ability, which have good photocatalytic performance, economic feasibility, sustainability and durability. We have described and compared the different forms of WO_3, synthetic binary or ternary heterojunctions, and other elements doped in different forms of WO_3. By modifying WO_3, the photocatalytic performance of WO_3 is improved to a certain extent. Studies have also shown that although doping a certain element promotes the photocatalytic performance of WO_3, the morphological structure of WO_3 has a greater effect on degradation wastewater ability than the supported cocatalyst. Therefore, there is still much space for improving the performance of WO_3 photocatalyst.

(1) Surface modification and morphology control have been demonstrated that can improve the photocatalytic activity of WO_3 photocatalysts. But more simple and efficient method with low cost is necessary to be developed for its realistic employment.
(2) The combination of WO_3 with another semiconductor for the formation of heterojunction is a promising way to promote the photocatalytic performance. However, whether binary or ternary, or more complex composites of WO_3-based photocatalysts, the deep micro-scale photocatalytic mechanism analysis is still a challenge and the integration of experiment and computational could be a good entry point.
(3) Many publications have been focused on element doping and modification to enhance the photocatalytic properties of WO_3. In most cases, noble elements or metals have been utilized, which increases the cost of materials and hinders its practical application. So highly efficient cheap metal elements or non-metallic elements modification method are urgently needed.
(4) Surface defect or vacancy is a very novel and effective methods in the study of other photocatalysts. However, about WO_3, relative studies are scarce, so some interests should be focused on this field of WO_3, which would be very efficient in further improving the photocatalytic activity of WO_3-based materials.

Acknowledgements

The study was financially supported by the National Natural Science Foundation of China (Grant No.51909089), Natural Science Foundation of Hunan Province, China (Grant No. 2020JJ5252), China Postdoctoral Science Foundation (Grant No. 2019M662781), Research Foundation of Education Bureau of Hunan Province, China (Grant No. 20B304), Science Foundation for Young Scholars of Hunan Agricultural University (19QN35), and Hunan Provincial Innovation Foundation for Postgraduate (CX20200663).

References

[1] Prashant V.Kamat, Kei Murakoshi, Yuji Wada et al (2000) Chapter 6—Semiconductor nanoparticles. Handbook of

Nanostructured Materials and Nanotechnolgy 3: 291–344. https://doi.org/10.1016/B978-012513760-7/50037-X.

[2] Apichon Watcharenwong, Wilaiwan Chanmanee, Norma R. de Tacconi et al (2008) Anodic growth of nanoporous WO_3 films: Morphology, photoelectrochemical response and photocatalytic activity for methylene blue and hexavalent chrome conversion. J Electroanal Chem 612:112–120. https://doi.org/10.1016/j.jelechem.2007.09.030.

[3] Zheng Q, Durkin DP, Elenewski JE et al (2016) Visible-light-responsive graphitic carbon nitride: rational design and photocatalytic aapplications for water treatment Environ Sci Technol 50:12938–12948. https://doi.org/10.1021/acs.est.6b02579

[4] Chao Zhen, Tingting Wu, Runze Chen et al. (2019) Strategies for modifying TiO_2 bbased electron transport layers to boost Perovskite solar cells. ACS Sustain Chem Eng 7:4586–4618. https://doi.org/10.1021/acssuschemeng.8b06580.

[5] Fujishima A, Honda K (1972) Electrochemical photolysis of water at a semiconductor electrode. Nature 238:37–38

[6] Gongming Wang, Hanyu Wang, Yichuan Ling et al (2011) Hydrogen-treated TiO_2 nanowire arrays for photoelectrochemical water splitting. Nano Lett 11: 3026–33. https://doi.org/10.1021/nl201766h.

[7] Linsebigler AL, Guangquan Lu, Yates JT (1995) Photocatalysis on TiOn surfaces: principles, mmechanisms, and selected results. Chem Rev 95:735–758

[8] Butler MA, Nasby RD, Quinn RK (1976) Tungsten triodide as an electrode for photoelectrolysis of water. Solid State Commun

[9] Ping-Quan Wang, Yang Bai, Ping-Ya Luo et al (2013) Graphene–WO_3 nanobelt composite: elevated conduction band toward photocatalytic reduction of CO_2 into hydrocarbon fuels. Catalysis Commun 38: 82–85. https://doi.org/10.1016/j.catcom.2013.04.020.

[10] Senlin Deng, Zebin Yang, Guojun Lv et al (2019) WO_3 nanosheets/g-C_3N_4 nanosheets' nanocomposite as an effective photocatalyst for degradation of rhodamine B.. Appl Phys A Mater Sci Process 125. https://doi.org/10.1007/s00339-018-2331-9.

[11] Suk Joon Hong, Hwichan Jun, Pramod H. Borse et al (2009) Size effects of WO_3 nanocrystals for photooxidation of water in particulate suspension and photoelectrochemical film systems. Int J Hydrogen Energy 34: 3234–3242. https://doi.org/10.1016/j.ijhydene.2009.02.006.

[12] Zheng H, Jian Zhen Ou, Strano MS et al (2011) Nanostructured tungsten oxide—properties, synthesis, and applications. Adv Func Mater 21:2175–2196. https://doi.org/10.1002/adfm.201002477

[13] Bilal Ahmed, Animesh K. Ojha, Ajeet Singh et al (2018) Well-controlled in-situ growth of 2D WO_3 rectangular sheets on reduced graphene oxide with strong photocatalytic and antibacterial properties. J Hazard Mater 347: 266–278. https://doi.org/10.1016/j.jhazmat.2017.12.069.

[14] Gondal MA, Seddigi Z (2006) Laser-induced photo-catalytic removal of phenol using *n*-type WO_3 semiconductor catalyst. Chem Phys Lett 417: 124–127. https://doi.org/10.1016/j.cplett.2005.09.115.

[15] Deng Y, Li Z, Tang R et al (2020) What will happen when microorganisms "meet" photocatalysts and photocatalysis? Environ Sci Nano 7:702–723. https://doi.org/10.1039/c9en01318k

[16] Tahir MB, Ali S, Rizwan M (2019) A review on remediation of harmful dyes through visible light-driven WO_3 photocatalytic nanomaterials. Int J Environ Sci Technol 16:4975–4988. https://doi.org/10.1007/s13762-019-02385-5.

[17] Longbo Jiang, Xingzhong Yuan, Guangming Zeng et al (2018) In-situ synthesis of direct solid-state dual Z-scheme WO_3/g-C_3N_4/Bi_2O_3 photocatalyst for the degradation of refractory pollutant. Appl Catal B Environ 227:376–385. https://doi.org/10.1016/j.apcatb.2018.01.042.

[18] Ying Peng Xie, Gang Liu, Lichang Yin et al (2012) Crystal facet-dependent photocatalytic oxidation and reduction reactivity of monoclinic WO_3 for solar energy conversion. J Mater Chem 22. https://doi.org/10.1039/c2jm16178h.

[19] Mousa Farhadian, Parvaneh Sangpour, Ghader Hosseinzadeh (2015) Morphology dependent photocatalytic activity of WO_3 nanostructures. J Energy Chem 24:171–177. https://doi.org/10.1016/s2095-4956(15)60297-2.

[20] Xiaoqiang An, Jimmy C. Yu, Yu Wang et al (2012) WO_3 nanorods/graphene nanocomposites for high-efficiency visible-light-driven photocatalysis and NO_2 gas sensing. J Mater Chem 22. https://doi.org/10.1039/c2jm16709c.

[21] Jinguo Wang, Zimei Chen, Guangjun Zhai et al (2018) Boosting photocatalytic activity of WO_3 nanorods with tailored surface oxygen vacancies for selective alcohol oxidations. Appl Surface Sci 462:760–771. https://doi.org/10.1016/j.apsusc.2018.08.181.

[22] Shunyu Yao, Fengyu Qu, Gang Wang et al (2017) Facile hydrothermal synthesis of WO_3 nanorods for photocatalysts and supercapacitors. J Alloys Compounds 724:695–702. https://doi.org/10.1016/j.jallcom.2017.07.123.

[23] Bilal Ahmed, Sumeet Kumar, Animesh K. Ojha et al (2017) Facile and controlled synthesis of aligned WO_3 nanorods and nanosheets as an efficient photocatalyst material. Spectrochim Acta A Molecular Biomolecular Spectroscopy 175:250–261. https://doi.org/10.1016/j.saa.2016.11.044.

[24] Ofori FA, Sheikh FA, Appiah-Ntiamoah R et al (2015) A simple method of electrospun tungsten trioxide nanofibers with enhanced visible-light photocatalytic activity. Nano-Micro Lett 7:291–297. https://doi.org/10.1007/s40820-015-0042-8

[25] Xiongwen Lou, Huachun Zhang (2003) An inorganic route for controlled synthesis of $W_{18}O_{49}$. Nanorods Inorganic Chem 42:6169–6171. https://doi.org/10.1021/ic034771q.

[26] Su J, Feng X, Sloppy JD et al (2011) Vertically aligned WO_3 nanowire arrays grown directly on transparent conducting oxide coated glass: synthesis and photoelectrochemical properties. Nano Lett 11:203–208. https://doi.org/10.1021/nl1034573.

[27] Zhao Z-G, Miyauchi M (2008) Nanoporous-walled tungsten oxide nanotubes as highly active visible-light-driven photocatalysts. Angew Chem 120:7059–7163. https://doi.org/10.1002/anie.200802207

[28] Xiaoqing Gao, Chao Yang, Feng Xiao et al (2012) WO_3-$0.33H_2O$ nanoplates: hydrothermal synthesis, photocatalytic and gas-sensing properties.Mater Lett 84:151–153. https://doi.org/10.1016/j.matlet.2012.06.078.

[29] Xiaoqing Gao, Xintai Su, Chao Yang et al (2013) Hydrothermal synthesis of WO_3 nanoplates as highly sensitive cyclohexene sensor and high-efficiency MB photocatalyst. Sensors Actuators B Chem 181:537–543. https://doi.org/10.1016/j.snb.2013.02.031.

[30] Mohite SV, Ganbavle VV, Rajpure KY (2016) Solar photoelectrocatalytic activities of rhodamine-B using sprayed WO_3 photoelectrode. J Alloys Compounds 655:106–113. https://doi.org/10.1016/j.jallcom.2015.09.154.

[31] Zhang Y-Q, Li X-H, Lü J et al (2014) A ternary TiO2/WO3/graphene nanocomposite adsorbent: facile preparation and efficient removal of Rhodamine B. Int J Minerals Metal Mater 21:813–819. https://doi.org/10.1007/s12613-014-0975-9

[32] Jian Yi Luo, Zhi Cao, Feng Chen et al. (2013) Strong aggregation adsorption of methylene blue from water using amorphous WO_3 nanosheets Applied Surface Science 287: 270–275. https://doi.org/10.1016/j.apsusc.2013.09.139.

[33] Yan Liang, Yong Yang, Chengwu Zou et al (2019) 2D ultra-thin WO_3 nanosheets with dominant {002} crystal facets for high-performance xylene sensing and methyl orange photocatalytic degradation. J Alloys Compounds 783: 848–854. https://doi.org/10.1016/j.jallcom.2018.12.384.

[34] Wu J, Qiao P, Li H et al (2019) Surface-oxygen vacancy defect-promoted electron-hole separation of defective tungsten trioxide ultrathin nanosheets and their enhanced solar-driven photocatalytic performance. J Colloid Interface Sci 557:18–27. https://doi.org/10.1016/j.jcis.2019.09.006

[35] Xiaoguang Wang, Minghui Sun, Muthu Murugananthan et al (2020) Electrochemically self-doped WO_3/TiO_2 nanotubes for photocatalytic degradation of volatile organic compounds. Appl Catal B Environ 260. https://doi.org/10.1016/j.apcatb.2019.118205.

[36] Jiaguo Yu, Qi L, Cheng B et al (2008) Effect of calcination temperatures on microstructures and photocatalytic activity of tungsten trioxide hollow microspheres. J Hazard Mater 160:621–628. https://doi.org/10.1016/j.jhazmat.2008.03.047

[37] Li Q-H, Wang L-M, Chu D-Q et al (2014) Cylindrical stacks and flower-like tungsten oxide microstructures: controllable synthesis and photocatalytic properties. Ceram Int 40:4969–4973. https://doi.org/10.1016/j.ceramint.2013.09.115

[38] Dandan Xu, Tengfei Jiang, Dejun Wang et al (2014) pH-Dependent assembly of Tungsten oxide three-dimensional architectures and their application in photocatalysis. ACS Appl Mater Interfaces 6:9321–7. https://doi.org/10.1021/am501651m.

[39] Zhenfeng Wang, Deqing Chu, Limin Wang et al (2017) EDTA-assisted synthesis of camellia-like WO_3 ·$0.33H_2O$ architectures with enhanced visible-light-driven photocatalytic activity. Catalysis Commun 88:1–4. https://doi.org/10.1016/j.catcom.2016.09.021.

[40] Haitao Wang, Huifang Yang, Deqing Chu et al (2017) Synthesis of 3D hierarchical WO_3·$0.33H_2O$ microsphere architectures with enhanced visible-light-driven photocatalytic activity. Mater Lett 193:5–8. https://doi.org/10.1016/j.matlet.2017.01.048.

[41] Liang Zhang, Xincun Tang, Zhouguang Lu et al (2011) Facile synthesis and photocatalytic activity of hierarchical WO_3 core–shell microspheres. Appl Surface Sci 258:1719–1724. https://doi.org/10.1016/j.apsusc.2011.10.022.

[42] Shunyu Yao, Xu Zhang, Fengyu Qu et al (2016) Hierarchical WO_3 nanostructures assembled by nanosheets and their applications in wastewater purification. J Alloys ompounds 689:570–574. https://doi.org/10.1016/j.jallcom.2016.08.025.

[43] Chen Di, Ye J (2008) Hierarchical WO_3 hollow shells: dendrite, sphere, dumbbell, and their photocatalytic properties. Adv Func Mater 18:1922–1928. https://doi.org/10.1002/adfm.200701468

[44] Gang Liu, Jimmy C. Yu, Gao Qing (Max), Lu et al. (2011) Crystal facet engineering of semiconductor photocatalysts: motivations, advances and unique properties. Chem Commun 47:6763–6783. https://doi.org/10.1039/c1cc10665a.

[45] Jin Yang, Jiadong Xiao, Hongbin Cao et al (2018) The role of ozone and influence of band structure in WO_3

photocatalysis and ozone integrated process for pharmaceutical wastewater treatment. J Hazard Mater 360:481–489. https://doi.org/10.1016/j.jhazmat.2018.08.033.

[46] Siyu Zhang, Hui Li, Zhifeng Yang (2017) Controllable synthesis of WO_3 with different crystalline phases and its applications on methylene blue removal from aqueous solution. J Alloys Compounds 722:555–563. https://doi.org/10.1016/j.jallcom.2017.06.095.

[47] Reza Abazari, Ali Reza Mahjoub, Lotf Ali Saghatforoush et al (2014) Characterization and optical properties of spherical WO_3 nanoparticles synthesized via the reverse microemulsion process and their photocatalytic behavior. Mater Lett 133:208–211. https://doi.org/10.1016/j.matlet.2014.07.032.

[48] Jianhua Huang, Liang Xiao, Xiaolong Yang (2013) WO_3 nanoplates, hierarchical flower-like assemblies and their photocatalytic properties. Mater Res Bull 48:2782–2785. https://doi.org/10.1016/j.materresbull.2013.04.022.

[49] Xiao-Ju Wen, Cheng-Gang Niu, Lei Zhang et al (2018) A novel Ag_2O/CeO_2 heterojunction photocatalysts for photocatalytic degradation of enrofloxacin: possible degradation pathways, mineralization activity and an in depth mechanism insight. Appl Catal B Environ 221:701–714. https://doi.org/10.1016/j.apcatb.2017.09.060.

[50] Weilai Yu, Junxiang Chen, Tongtong Shang et al (2017) Direct Z-scheme g-C_3N_4/WO_3 photocatalyst with atomically defined junction for H2 production. Appl Catal B Environ 219:693–704. https://doi.org/10.1016/j.apcatb.2017.08.018.

[51] Deng Y, Feng C, Tangb L et al (2020) Ultrathin low dimensional heterostructure composites with superior photocatalytic activity: Insight into the multichannel charge transfer mechanism. Chem Eng J 393:124718. https://doi.org/10.1016/j.cej.2020.124718

[52] Liying Huang, Hui Xu, Yeping Li et al (2013) Visible-light-induced WO_3/g-C_3N_4 composites with enhanced photocatalytic activity. Dalton Trans 42:8606–8616. https://doi.org/10.1039/c3dt00115f.

[53] Guochang Chen, Shicong Bian, Cun-Yue Guo et al (2019) Insight into the Z-scheme heterostructure WO_3/g-C_3N_4 for enhanced photocatalytic degradation of methyl orange. Mater Lett 236: 596–599. https://doi.org/10.1016/j.matlet.2018.11.010.

[54] Jikai Yang, Xintong Zhang, Hong Liu et al.(2013) Heterostructured TiO_2/WO_3 porous microspheres: preparation, characterization and photocatalytic properties. Catal Today 201:195–202. https://doi.org/10.1016/j.cattod.2012.03.008.

[55] Di Liberto G, Tosoni S, Pacchioni G (2019) Theoretical treatment of semiconductor heterojunctions for photocatalysis: the $WO_3/BiVO_4$ interface. J Phys Condensed Matter 31:434001. https://doi.org/10.1088/1361-648X/ab2fa4.

[56] Ashok Kumar KV, Chandana L, Ghosal P et al (2018) Simultaneous photocatalytic degradation of p-cresol and Cr (VI) by metal oxides supported reduced graphene oxide. Molecular Catal 451:87–95. https://doi.org/10.1016/j.mcat.2017.11.014.

[57] Jeevitha G, Abhinayaa R, Mangalaraj D et al (2018) Tungsten oxide-graphene oxide (WO_3-GO) nanocomposite as an efficient photocatalyst, antibacterial and anticancer agent. J Phys Chem Solids 116:137–147. https://doi.org/10.1016/j.jpcs.2018.01.021.

[58] Tao Jiang, Ling Cheng, Yingchun Han et al (2020) One-pot hydrothermal synthesis of Bi_2O3-WO_3 p-n heterojunction film for photoelectrocatalytic degradation of norfloxacin. Separation Purification Technol 238:116428. https://doi.org/10.1016/j.seppur.2019.116428.

[59] Minghuan Gao, Lisha You, Linna Guo et al (2019) Fabrication of a novel polyhedron-like WO_3/Ag_2CO_3 p-n junction photocatalyst with highly enhanced photocatalytic activity. J Photochem Photobiol A Chem 374:206–217. https://doi.org/10.1016/j.jphotochem.2019.01.022.

[60] Jin Luo, Xiaosong Zhou, Lin Ma et al (2015) Enhanced visible-light-driven photocatalytic activity of WO_3/BiOI heterojunction photocatalysts. J Molecular Catal A Chem 410:168–176. https://doi.org/10.1016/j.molcata.2015.09.019.

[61] Deng Y, Tang L, Feng C et al (2018) Insight into the dual-channel charge-charrier transfer path for nonmetal plasmonic tungsten oxide based composites with boosted photocatalytic activity under full-spectrum light. Appl Catal B 238:225–237. https://doi.org/10.1016/j.apcatb.2018.04.075

[62] Hui Xu, Liang Liu, Xiaojie She et al (2016) WO_3 nanorod photocatalysts decorated with few-layer g-C_3N_4 nanosheets: controllable synthesis and photocatalytic mechanism research. RSC Adv 6:80193–80200. https://doi.org/10.1039/c6ra12861k.

[63] Junwei Fu, Quanlong Xu, Jingxiang Low et al (2019) Ultrathin 2D/2D WO_3/g-C_3N_4 step-scheme H_2-production photocatalyst. Appl Catal B Environ 243:556–565. https://doi.org/10.1016/j.apcatb.2018.11.011.

[64] Tao Pan, Dongdong Chen, Weicheng Xu et al (2020) Anionic polyacrylamide-assisted construction of thin 2D-2D WO_3/g-C_3N_4 Step-scheme heterojunction for enhanced tetracycline degradation under visible light irradiation.

J Hazard Mater 393:122366. https://doi.org/10.1016/j.jhazmat.2020.122366.

[65] Fei He, Aiyun Meng, Bei Cheng et al (2020) Enhanced photocatalytic H_2-production activity of WO_3/TiO_2 step-scheme heterojunction by graphene modification. Chin J Catal 41:9–20. https://doi.org/10.1016/s1872-2067(19)63382-6.

[66] Pengfei Xia, Shaowen Cao, Bicheng Zhu et al (2020) Designing a 0D/2D S-Scheme heterojunction over polymeric carbon nitride for visible-light photocatalytic inactivation of bacteria. Angewandte Chem Int Edition. https://doi.org/10.1002/anie.201916012.

[67] Jingxiang Low, Jiaguo Yu, Mietek Jaroniec et al (2017) Heterojunction photocatalysts. Adv Mater 29. https://doi.org/10.1002/adma.201601694.

[68] Hao Zhang, Xiaojun Lv, Yueming Li et al (2010) P25-graphene composite as a high performance photocatalyst. ACS Nano 4:380–386. https://doi.org/10.1021/nn901221k.

[69] He Guo, Nan Jiang, Huijuan Wang et al. (2019) Pulsed discharge plasma assisted with graphene-WO_3 nanocomposites for synergistic degradation of antibiotic enrofloxacin in water Chemical Engineering Journal 372: 226–240. https://doi.org/10.1016/j.cej.2019.04.119.

[70] Lu Gan, Lijie Xu, Songmin Shang et al (2016) Visible light induced methylene blue dye degradation photo-catalyzed by WO_3/graphene nanocomposites and the mechanism. Ceramics Int 42:15235–15241. https://doi.org/10.1016/j.ceramint.2016.06.160.

[71] Wenyu Zhu, Faqian Sun, Ronn Goei et al (2017) Facile fabrication of RGO-WO_3 composites for effective visible light photocatalytic degradation of sulfamethoxazole. Appl Catal B Environ 207:93–102. https://doi.org/10.1016/j.apcatb.2017.02.012.

[72] Jingjing Guo, Yao Li, Shenmin Zhu et al (2012) Synthesis of WO_3@Graphene composite for enhanced photocatalytic oxygen evolution from water. RSC Adv 2:1356–1363. https://doi.org/10.1039/c1ra00621e.

[73] Junqi Li, Zhenxing Liu, Zhenfeng Zhu (2015) Enhanced photocatalytic activity in $ZnFe_2O_4$–ZnO–Ag_3PO_4 hollow nanospheres through the cascadal electron transfer with magnetical separation. J Alloys Compounds 636:229–233. https://doi.org/10.1016/j.jallcom.2015.02.176.

[74] Yaocheng Deng, Lin Tang, Guangming Zeng et al (2017) Plasmonic resonance excited dual Z-scheme $BiVO_4$/Ag/Cu_2O nanocomposite: synthesis and mechanism for enhanced photocatalytic performance in recalcitrant antibiotic degradation. Environ Sci Nano 4:1494–1511. https://doi.org/10.1039/c7en00237h.

[75] Qian Zhou, Yun Song, Najun Li et al (2020) Direct Dual Z-Scheme Bi_2WO_6/GQDs/WO_3 inverse opals for enhanced photocatalytic activities under visible light. ACS Sustain Chem Eng 8:7921–7927. https://doi.org/10.1021/acssuschemeng.0c01548.

[76] Yee Wen Teh, Yien Wei Goh, Xin Ying Kong et al (2019) Fabrication of Bi_2WO_6/Cu/WO_3 Allsolid-State Z-scheme composite photocatalyst to improve CO_2 photoreduction under visible light irradiation. ChemCatChem 11: 6431–6438. https://doi.org/10.1002/cctc.201901653.

[77] Jiayi Chen, Xinyan Xiao, Yi Wang et al (2019) Ag nanoparticles decorated WO_3/g-C_3N_4 2D/2D heterostructure with enhanced photocatalytic activity for organic pollutants degradation. Appl Surface Sci 467–468:1000–1010. https://doi.org/10.1016/j.apsusc.2018.10.236.

[78] Xingzhong Yuan, Longbo Jiang, Xiaohong Chen et al (2017) Highly efficient visible-light-induced photoactivity of Z-scheme Ag_2CO_3/Ag/WO_3 photocatalysts for organic pollutant degradation. Environ Sci Nano 4:2175–2185. https://doi.org/10.1039/c7en00713b.

[79] Shanshan Ding, Mengshu Han, Yuxuan Dai et al (2019) Synthesis of Ag/AgBr/$Bi4O_5Br_2$ plasmonic heterojunction photocatalysts: elevated visible-light photocatalytic performance and Z-scheme. Mech ChemCatChem 11:1–16. https://doi.org/10.1002/cctc.201900529.

[80] Jiabai Cai, Xueqing Wu, Shunxing Li et al (2016) Synthesis of TiO_2@WO_3/Au nanocomposite hollow spheres with controllable size and high visible-light-driven photocatalytic activity. ACS Sustain Chem Eng 4:1581–1590. https://doi.org/10.1021/acssuschemeng.5b01511.

[81] Jun Zhang, Yun Guo, Yuhan Xiong et al (2017) An environmentally friendly Z-scheme WO_3/CDots/CdS heterostructure with remarkable photocatalytic activity and anti-photocorrosion performance. J Catal 356:1–13. https://doi.org/10.1016/j.jcat.2017.09.021.

[82] Fangjun Wu, Xin Li, Wei Liu et al (2017) Highly enhanced photocatalytic degradation of methylene blue over the indirect all-solid-state Z-scheme g-C_3N_4-RGO-TiO_2 nanoheterojunctions. Appl Surface Sci 405:60–70. https://doi.org/10.1016/j.apsusc.2017.01.285.

[83] Na Lu, Pu Wang, Yan Su et al (2019) Construction of Z-Scheme g-C_3N_4/RGO/WO_3 with in situ photoreduced graphene oxide as electron mediator for efficient photocatalytic degradation of ciprofloxacin .Chemosphere 215: 444–453. https://doi.org/10.1016/j.chemosphere.2018.10.065.

[84] Ahmad Beyhaqi, Qingyi Zeng, Sheng Chang et al (2020) Construction of g-C_3N_4/WO_3/MoS_2 ternary nanocomposite with enhanced charge separation and collection for efficient wastewater treatment under visible light. Chemosphere 247:125784. https://doi.org/10.1016/j.chemosphere.2019.125784.

[85] Huali Li, Yajie Chen, Wei Zhou et al (2019) $WO_3/BiVO_4$/BiOCl porous nanosheet composites from a biomass template for photocatalytic organic pollutant degradation. J Alloys Compounds 802:76–85. https://doi.org/10.1016/j.jallcom.2019.06.187.

[86] Hyoung-il Kim, Jungwon Kim, Wooyul Kim et al (2011) Enhanced photocatalytic and photoelectrochemical activity in the Ternary Hybrid of $CdS/TiO_2/WO_3$ through the Cascadal electron transfer. J Phys Chem C 115:9797–9805. https://doi.org/10.1021/jp1122823.

[87] Narges Omrani, Alireza Nezamzadeh-Ejhieh (2020) A comprehensive study on the enhanced photocatalytic activity of $Cu_2O/BiVO_4/WO_3$ nanoparticles. J Photochem Photobiol A Chem 389. https://doi.org/10.1016/j.jphotochem.2019.112223.

[88] Zhenfeng Zhu, Ying Yan, Junqi Li (2015) Preparation of flower-like BiOBr–WO_3–Bi_2WO_6 ternary hybrid with enhanced visible-light photocatalytic activity. J Alloys Compounds 651:184–192. https://doi.org/10.1016/j.jallcom.2015.08.137.

[89] Ming Yan, Yilin Wu, Fangfang Zhu et al (2016) The fabrication of a novel Ag_3VO_4/WO_3 heterojunction with enhanced visible light efficiency in the photocatalytic degradation of TC. Phys Chem Chem Phys 18:3308–3315. https://doi.org/10.1039/c5cp05599g.

[90] Shijie Li, Shiwei Hu, Wei Jiang et al. (2019) In situ construction of WO_3 nanoparticles decorated Bi_2MoO_6 microspheres for boosting photocatalytic degradation of refractory pollutants. J Colloid Interface Sci 556:335–344. https://doi.org/10.1016/j.jcis.2019.08.077.

[91] Priya A, Prabhakarn Arunachalam, Selvi A et al (2018) Synthesis of $BiFeWO_6/WO_3$ nanocomposite and its enhanced photocatalytic activity towards degradation of dye under irradiation of light. Colloids Surfaces A Physicochem Eng Aspects 559:83–91. https://doi.org/10.1016/j.colsurfa.2018.09.031.

[92] Shifu Chen, Yingfei Hu, Sugang Meng et al (2014) Study on the separation mechanisms of photogenerated electrons and holes for composite photocatalysts g-C_3N_4-WO_3. Appl Catal B Environ 150–151:564–573. https://doi.org/10.1016/j.apcatb.2013.12.053.

[93] Mahdi Karimi-Nazarabad, Elaheh K. Goharshadi (2017) Highly efficient photocatalytic and photoelectrocatalytic activity of solar light driven WO_3/g-C_3N_4 nanocomposite. Solar Energy Mater Solar Cells 160:484–493. https://doi.org/10.1016/j.solmat.2016.11.005.

[94] Manoj Pudukudy, Shaoyun Shan, Yingju Miao et al (2020) WO_3 nanocrystals decorated Ag_3PO_4 tetrapods as an efficient visible-light responsive Z-scheme photocatalyst for the enhanced degradation of tetracycline in aqueous medium. Colloids Surfaces A Physicochem Eng Aspects 589. https://doi.org/10.1016/j.colsurfa.2020.124457.

[95] Jinsuo Lu, Yujing Wang, Fei Liu et al (2017) Fabrication of a direct Z-scheme type WO_3/Ag_3PO_4 composite photocatalyst with enhanced visible-light photocatalytic performances. Appl Surface Sci 393:180–190. https://doi.org/10.1016/j.apsusc.2016.10.003.

[96] Xingchao Zhang, Ruoyu Zhang, Siying Niu et al (2019) Construction of core-shell structured WO_3@SnS_2 heterojunction as a direct Z-scheme photo-catalyst. J Colloid Interface Sci 554:229–238. https://doi.org/10.1016/j.jcis.2019.06.107.

[97] Jichao Zhu, Jie He, Lifang Hu et al (2019) All-solid-state Z-scheme WO_3/HTiNbO$_5$-NS heterojunctions with enhanced photocatalytic performance. J Solid State Chem 276:104–113. https://doi.org/10.1016/j.jssc.2019.04.026.

[98] Hanan H. Mohamed (2019) Rationally designed Fe_2O_3/GO/WO_3 Z-Scheme photocatalyst for enhanced solar light photocatalytic water remediation. J Photochem Photobiol A Chem 378:74–84. https://doi.org/10.1016/j.jphotochem.2019.04.023.

[99] Pingfan Xu, Siyi Huang, Minghua Liu et al (2019) Z-Schemed WO_3/rGO/$SnIn_4S_8$ Sandwich Nanohybrids for Efficient Visible Light Photocatalytic Water Purification Catalysts 9: https://doi.org/10.3390/catal9020187.

[100] Hameed A, Gondal MA, Yamani ZH (2004) Effect of transition metal doping on photocatalytic activity of WO_3 for water splitting under laser illumination: role of 3d-orbitals. Catalysis Commun 5:715–719. https://doi.org/10.1016/j.catcom.2004.09.002.

[101] Hui Song, Yaguang Li, Zirui Lou et al (2015) Synthesis of Fe-doped WO_3 nanostructures with high visible-light-driven photocatalytic activities. Appl Catal Environ 166–167:112–120. https://doi.org/10.1016/j.apcatb.2014.11.020.

[102] Vijay Luxmi, Ashavani Kumar (2019) Enhanced photocatalytic performance of m-WO_3 and m-Fe-doped WO_3 cuboids synthesized via sol-gel approach using egg albumen as a solvent Materials Science in Semiconductor Processing 104: https://doi.org/10.1016/j.mssp.2019.104690.

[103] Chao Min Teh, Abdul Rahman Mohamed (2011) Roles of titanium dioxide and ion-doped titanium dioxide on photocatalytic degradation of organic pollutants (phenolic compounds and dyes) in aqueous solutions: a review. J Alloys Compounds 509:1648–1660. https://doi.org/10.1016/j.jallcom.2010.10.181.

[104] Bilal Tahir M, Sagir M (2019) Carbon nanodots and rare metals (RM = La, Gd, Er) doped tungsten oxide nanostructures for photocatalytic dyes degradation and hydrogen

production. Separation Purification Technol 209:94–102. https://doi.org/10.1016/j.seppur.2018.07.029.

[105] Liu H, Peng T, Ke D et al (2007) Preparation and photocatalytic activity of dysprosium doped tungsten trioxide nanoparticles. Mater Chem Phys 104:377–383. https://doi.org/10.1016/j.matchemphys.2007.03.028

[106] Xiying Zhu, Pan Zhang, Bin Li et al (2017) Preparation, characterization and photocatalytic properties of La/WO_3 composites. J Mater Sci Mater Electron 28:12158–12167. https://doi.org/10.1007/s10854-017-7030-3.

[107] Cong Wang, Lin Cao (2011) Preparation, spectral characteristics and photocatalytic activity of Eu^{3+}-doped WO_3 nanoparticles. J Rare Earths 29:727–731. https://doi.org/10.1016/s1002-0721(10)60531-5.

[108] Mohite SV, Ganbavle VV, Rajpure Ky (2017) Photoelectrocatalytic activity of immobilized Yb doped WO_3 photocatalyst for degradation of methyl orange dye. J Energy Chem 26:440–447. https://doi.org/10.1016/j.jechem.2017.01.001.

[109] Girish Kumar S, Koteswara Rao KSR (2015) Tungsten-based nanomaterials (WO_3 & Bi_2WO_6): Modifications related to charge carrier transfer mechanisms and photocatalytic applications. Appl Surface Sci 355:939–958. https://doi.org/10.1016/j.apsusc.2015.07.003.

[110] Guodong Chen, Qi Wang, Zhilin Zhao et al (2020) Synthesis and photocatalytic activity study of S-doped WO_3 under visible light irradiation. Environ Sci Pollut Res. https://doi.org/10.1007/s11356-020-07827-z.

[111] Yaocheng Deng, Lin Tang, Guangming Zeng et al (2017) Insight into highly efficient simultaneous photocatalytic removal of Cr(VI) and 2,4-diclorophenol under visible light irradiation by phosphorus doped porous ultrathin g-C_3N_4 nanosheets from aqueous media: Performance and reaction mechanism. Appl Catal B Environ 203:343–354. https://doi.org/10.1016/j.apcatb.2016.10.046.

[112] Fugui Han, Heping Li, Li Fu et al (2016) Synthesis of S-doped WO_3 nanowires with enhanced photocatalytic performance towards dye degradation. Chem Phys Lett 651:183–187. https://doi.org/10.1016/j.cplett.2016.03.017.

[113] Yuyang Liu, Ya Li, Wenzhang Li et al (2012) Photoelectrochemical properties and photocatalytic activity of nitrogen-doped nanoporous WO_3 photoelectrodes under visible light. Appl Surface Sci 258:5038–5045. https://doi.org/10.1016/j.apsusc.2012.01.080.

[114] Keyan Bao, Shaojie Zhang, Ping Ni et al (2020) Convenient fabrication of carbon doped WO_{3-x} ultrathin nanosheets for photocatalytic aerobic oxidation of amines. Catal Today 340:311–317. https://doi.org/10.1016/j.cattod.2018.11.013.

[115] Deng Y, Tang L, Feng C et al (2017) Construction of plasmonic Ag and nitrogen-doped Graphene quantum dots codecorated ultrathin graphitic carbon nitride nanosheet composites with enhanced photocatalytic activity: full-spectrum response ability and mechanism insight. ACS Appl Mater Interfaces 9:42816–42828. https://doi.org/10.1021/acsami.7b14541

[116] Mohammadi S, Sohrabi M, Golikand AN et al (2016) Preparation and characterization of zinc and copper co-doped WO_3 nanoparticles: Application in photocatalysis and photobiology. J Photochem Photobiol B Biol 61:217–21. https://doi.org/10.1016/j.jphotobiol.2016.05.020.

[117] Xu Ying, Zhou Ying, Nie Guo Zheng et al (2018) Tailoring the photocatalytic activity of WO_3 by Nb-F codoping from first-principles calculations. Chin J Phys 56:2285–2290. https://doi.org/10.1016/j.cjph.2018.07.003.

[118] Tijani JO, Ugochukwu O, Fadipe LA et al (2019) Photocatalytic degradation of local dyeing wastewater by iodine-phosphorus co-doped tungsten trioxide nanocomposites under natural sunlight irradiation. J Environ Manage 236:519–533. https://doi.org/10.1016/j.jenvman.2019.02.027

[119] Gondal MA, Bagabas A, Dastageer A et al (2010) Synthesis, characterization, and antimicrobial application of nano-palladium-doped nano-WO_3. J Molecular Catal A Chem 323:78–83. https://doi.org/10.1016/j.molcata.2010.03.019.

[120] Jijin Mai, Yanxiong Fang, Jincheng Liu et al. (2019) Simple synthesis of WO_3-Au composite and their improved photothermal synergistic catalytic performance for cyclohexane oxidation Molecular Catalysis 473: https://doi.org/10.1016/j.mcat.2019.04.018.

[121] Jungwon Kim, Chul Wee Lee, Wonyong Choi (2010) Platinized WO_3 as an environmental photocatalyst that generates OH radicals under visible light. Environ Sci Technol 44:6849–6854. https://doi.org/10.1021/es101981r.

[122] Wicaksana Y, Liu S, Scott J et al (2014) Tungsten trioxide as a visible light photocatalyst for volatile organic carbon removal. Molecules 19:17747–17762. https://doi.org/10.3390/molecules191117747

[123] Mohsen Khajeh Aminian, Jinhua Ye (2011) Morphology influence on photocatalytic activity of tungsten oxide loaded by platinum nanoparticles. J Mater Res 25:141–148. https://doi.org/10.1557/jmr.2010.0021

[124] Qamar M, Yamani ZH, Gondal MA et al (2011) Synthesis and comparative photocatalytic activity of Pt/WO_3 and Au/WO_3 nanocomposites under sunlight-type excitation. Solid State Sci 13:1748–1754. https://doi.org/10.1016/j.solidstatesciences.2011.07.002.

[125] Wenyu Zhu, Jincheng Liu, Shuyan Yu et al (2016) Ag loaded WO_3 nanoplates for efficient photocatalytic degradation of sulfanilamide and their bactericidal effect under visible light irradiation. J Hazard Mater 318:407–416. https://doi.org/10.1016/j.jhazmat.2016.06.066.

[126] Faisal Mehmood, Javed Iqbal, Tariq Jan et al (2017) Structural, photoluminescence, electrical, anti cancer and visible light driven photocatalytic characteristics of Co doped WO_3 nanoplates. Vibrational Spectroscopy 93:78–89. https://doi.org/10.1016/j.vibspec.2017.09.005.

[127] Faisal Mehmood, Javed Iqbal, Ismail M et al (2018) Ni doped WO_3 nanoplates: an excellent photocatalyst and novel nanomaterial for enhanced anticancer activities. J Alloys Compounds 746:729–738. https://doi.org/10.1016/j.jallcom.2018.01.409.

[128] Dhanalakshmi M, Lakshmi Prabavathi S, Saravanakumar K et al (2020) Iridium nanoparticles anchored WO_3 nanocubes as an efficient photocatalyst for removal of refractory contaminants (crystal violet and methylene blue). Chem Phys Lett 745. https://doi.org/10.1016/j.cplett.2020.137285.

[129] Adel A. Ismail, M. Faisal, Adel Al-Haddad (2018) Mesoporous WO_3-graphene photocatalyst for photocatalytic degradation of Methylene Blue dye under visible light illumination. J Environ Sci 66:328–337. https://doi.org/10.1016/j.jes.2017.05.001.